Article

Cell Reports

Fast Regulation of $GABA_AR$ Diffusion Dynamics by Nogo-A Signaling

Graphical Abstract

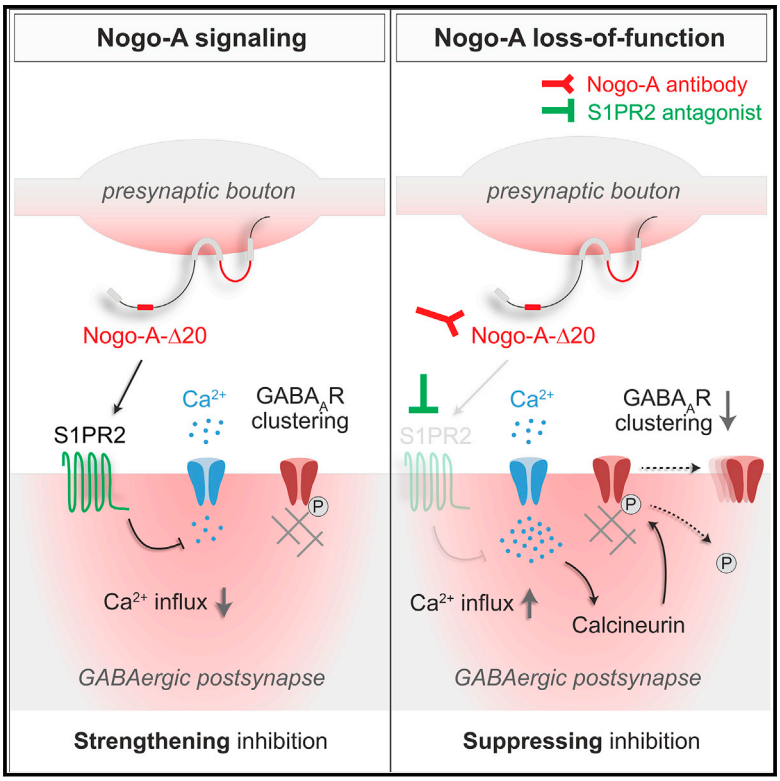

Highlights

- Nogo-A signaling strengthens inhibitory synaptic transmission within minutes
- Nogo-A signaling restricts $GABA_AR$ diffusion and promotes synaptic localization
- S1PR2 but not NgR1 mediates the effect of Nogo-A at inhibitory synapses
- These effects of Nogo-A occur in a Ca^{2+}- and calcineurin-dependent manner

Authors

Steffen Fricke, Kristin Metzdorf, Melanie Ohm, Stefan Haak, Martin Heine, Martin Korte, Marta Zagrebelsky

Correspondence

m.zagrebelsky@tu-bs.de

In Brief

Fricke et al. explore the molecular mechanisms regulating the strength of inhibitory synaptic transmission and the $GABA_AR$ localization at inhibitory synapses. Nogo-A/S1PR2 signaling rapidly strengthens inhibitory synaptic transmission in the hippocampus, limits $GABA_AR$ diffusion dynamics, and promotes $GABA_AR$ clustering at synapses in a Ca^{2+}- and calcineurin-dependent manner.

Fricke et al., 2019, Cell Reports *29*, 671–684
October 15, 2019
https://doi.org/10.1016/j.celrep.2019.09.015

CellPress

Cell Reports
Article

Fast Regulation of $GABA_AR$ Diffusion Dynamics by Nogo-A Signaling

Steffen Fricke,[1,5] Kristin Metzdorf,[1,5] Melanie Ohm,[1] Stefan Haak,[1] Martin Heine,[2,4] Martin Korte,[1,3] and Marta Zagrebelsky[1,6,*]
[1]Zoological Institute, Division of Cellular Neurobiology, TU Braunschweig, Braunschweig 38108, Germany
[2]Molecular Physiology Group, Leibniz Institute of Neurobiology, Magdeburg 39118, Germany
[3]Helmholtz Centre for Infection Research, AG NIND, Inhoffenstr. 7, Braunschweig 38124, Germany
[4]Functional Neurobiology, Institute for Developmental Biology and Neurobiology, Johannes Gutenberg University, Mainz 55128, Germany
[5]These authors contributed equally
[6]Lead Contact
*Correspondence: m.zagrebelsky@tu-bs.de
https://doi.org/10.1016/j.celrep.2019.09.015

SUMMARY

Precisely controlling the excitatory and inhibitory balance is crucial for the stability and information-processing ability of neuronal networks. However, the molecular mechanisms maintaining this balance during ongoing sensory experiences are largely unclear. We show that Nogo-A signaling reciprocally regulates excitatory and inhibitory transmission. Loss of function for Nogo-A signaling through S1PR2 rapidly increases $GABA_AR$ diffusion, thereby decreasing their number at synaptic sites and the amplitude of GABAergic mIPSCs at CA3 hippocampal neurons. This increase in $GABA_AR$ diffusion rate is correlated with an increase in Ca^{2+} influx and requires the calcineurin-mediated dephosphorylation of the γ2 subunit at serine 327. These results suggest that Nogo-A signaling rapidly strengthens inhibitory GABAergic transmission by restricting the diffusion dynamics of $GABA_ARs$. Together with the observation that Nogo-A signaling regulates excitatory transmission in an opposite manner, these results suggest a crucial role for Nogo-A signaling in modulating the excitation and inhibition balance to restrict synaptic plasticity.

INTRODUCTION

As inhibitory synaptic transmission plays a crucial role in shaping the function of the neuronal network, adjustments in its strength represent a key regulatory mechanism for different brain processes, such as learning and memory (Barron et al., 2017; Isaacson and Scanziani, 2011; Maffei, 2011). The strength of inhibitory GABAergic synapses is defined by the number of postsynaptic chloride-selective ionotropic type A GABA receptors ($GABA_ARs$) (Kilman et al., 2002; Moss and Smart, 2001), depending on the rate of their insertion and removal and their local lateral diffusion (Choquet and Triller, 2013). Thus, the exchange of surface receptors between synaptic and extrasynaptic sites and their confinement are among the most important determinants of the strength of GABAergic synapses. In hippocampal neurons, fast GABAergic inhibition is regulated through the control of $GABA_AR$ diffusion in an *N*-methyl D-aspartic acid receptor (NMDAR)-dependent and a Ca^{2+}-dependent manner. Sustained Ca^{2+} influx via NMDARs results in a decrease in $GABA_ARs$ at synapses and an increase in their lateral diffusion due to the calcineurin (CaN)-mediated dephosphorylation of their γ2 subunit at serine 327 (Ser327; Bannai et al., 2009; Luscher et al., 2011; Muir et al., 2010). While extracellular signaling increasing $GABA_AR$ diffusion and thus suppressing inhibitory transmission have been identified (e.g., brain-derived neurotrophic factor [BDNF] signaling and increased neuronal activity [Brünig et al., 2001; Goodkin et al., 2005]), little is known about molecules limiting their diffusion and thereby strengthening inhibition. Addressing this question is crucial for understanding how the appropriate excitation and inhibition balance in the brain is maintained, allowing the tight regulation of plastic processes.

Nogo-A signaling via its receptors NgR1, S1PR2, and PirB is known to limit neural plasticity in the mature CNS (Schwab and Strittmatter, 2014). Originally described as a myelin-derived inhibitor for neurite outgrowth and regeneration (Caroni et al., 1988; Chen et al., 2000; Fournier et al., 2001; GrandPré et al., 2002; Schnell and Schwab, 1990), Nogo-A has also been found to be expressed by subsets of neurons in CNS areas of high plasticity such as the hippocampus (Huber et al., 2002; Josephson et al., 2001; Liu et al., 2003; Zagrebelsky et al., 2010), where it localizes at synapses (Lee et al., 2008). Moreover, Nogo-A signaling restricts structural and functional activity-dependent synaptic plasticity in the intact adult brain (Akbik et al., 2013; Delekate et al., 2011; Iobbi et al., 2017; Karlsson et al., 2016; Kellner et al., 2016; Kempf et al., 2014; Raiker et al., 2010; Syken et al., 2006; Wills et al., 2012; Zagrebelsky et al., 2010; Zemmar et al., 2014, 2018). Among the molecular mechanisms mediating its ability to restrict synaptic plasticity, Nogo-A signaling has been shown to prevent α-amino-3-hydroxy-5-methyl-4-isoxazole propionic acid receptor (AMPAR) insertion at synapses under basal conditions and upon the induction of long-term potentiation (Kellner et al., 2016). Moreover, the deletion of NgR1 results in increased adult neural plasticity by facilitating

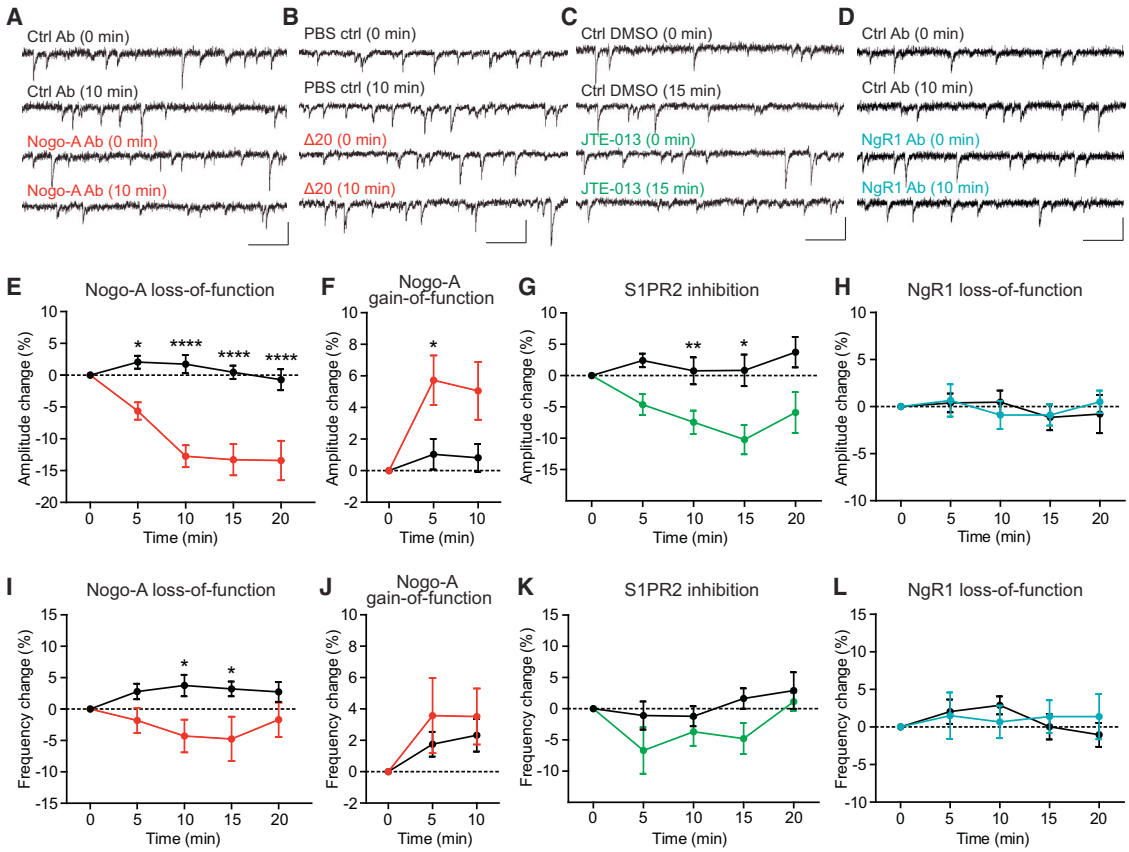

Figure 1. Nogo-A Strengthens Inhibitory Synaptic Transmission via the S1PR2

(A–D) mIPSC recordings in organotypic hippocampal cultures before and after Nogo-A loss-of-function (A, red), Nogo-A gain of function (B, red), S1PR2 inhibition (C, green), NgR1 loss of function (D, blue), and the respective controls (black). Scale bars, 20 pA vertical and 200 ms horizontal.

(E–L) Normalized mIPSC amplitude and frequency change in percentage upon Nogo-A loss of function (E, ANOVA treatment, $p < 0.0001$, $F_{1,17} = 45.32$; I, ANOVA treatment, $p < 0.05$, $F_{1,17} = 6.834$, n = 9, red), Nogo-A gain of function (F, ANOVA treatment, $p < 0.05$, $F_{1,21} = 7.905$; J, n = 11, red), S1PR2 inhibition (G, ANOVA treatment, $p < 0.001$, $F_{1,18} = 21.72$; K, ANOVA treatment, $p < 0.05$, $F_{1,18} = 6.365$, n = 11, green), NgR1 loss of function (H and L, n = 12, blue) and controls (E and I, n = 10; F and J, n = 12; G and K, n = 9; H and L, n = 13, black).

Values represent means ± SEMs. *$p < 0.05$, **$p < 0.01$, ****$p < 0.0001$.

experience-driven delivery of AMPARs at synapses (Jitsuki et al., 2016). These observations suggest that Nogo-A/NgR1 signaling restricts activity-dependent synaptic plasticity by regulating the strength of glutamatergic synaptic transmission. However, no studies so far have addressed a possible role of the Nogo-A signaling on inhibitory GABAergic transmission. We report that blocking Nogo-A signaling via the S1PR2 in pyramidal hippocampal neurons results in the rapid increase in $GABA_AR$ lateral motility associated with a decrease in their number at synapses, leading to a decrease in the amplitude of GABAergic miniature inhibitory postsynaptic currents (mIPSCs). We also found that the increase in $GABA_AR$ motility upon Nogo-A loss of function is correlated with an increase in Ca^{2+} transient amplitude and CaN-mediated dephosphorylation of the $GABA_AR$ γ2 subunit at Ser327. Thus, Nogo-A/S1PR2 signaling rapidly promotes inhibitory GABAergic transmission by modulating the diffusion dynamics of $GABA_ARs$ and thereby shifts the excitation and inhibition balance to restrict synaptic plasticity.

RESULTS

Nogo-A Strengthens Inhibitory Synaptic Transmission via the S1PR2

To test whether Nogo-A regulates inhibitory GABAergic synaptic transmission, mIPSCs of CA3 hippocampal neurons were recorded in mouse organotypic slice cultures using whole-cell voltage clamp. Acute loss of function for Nogo-A, by the application of function-blocking antibodies specific for the NiG-Δ20 inhibitory domain (11C7; Oertle et al., 2003), resulted in a rapid significant decrease in the normalized mIPSC amplitude starting 5 min after antibody application and reaching a reduction of ~15% compared to controls (Figures 1A and 1E; 5 min: $p < 0.05$; 10–20 min: $p < 0.0001$; Figure S1A; Table S1). The normalized mIPSC frequency was significantly reduced up to ~10% at 10 and 15 min after Nogo-A blocking antibody application relative to controls (Figures 1A and 1I; 10 and 15 min: $p < 0.05$; Figure S1D; Table S1). Next, a gain-of-function approach for the Nogo-A NiG-Δ20 domain, by applying the soluble Δ20

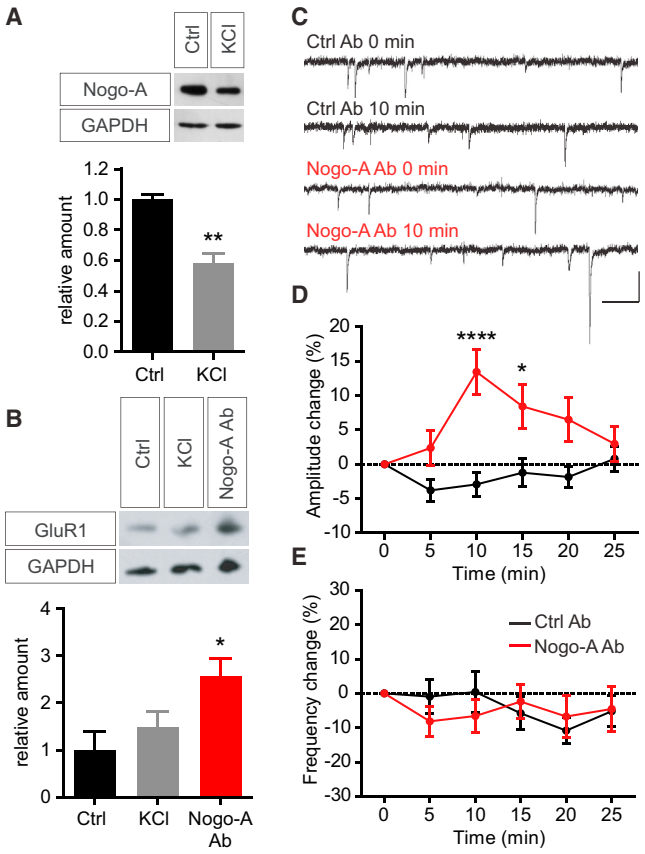

Figure 2. Activity-Dependent Localization of Nogo-A at Synapses

(A) Western blot for Nogo-A and glyceraldehyde 3-phosphate dehydrogenase (GAPDH) in synaptosomes from acute hippocampal slices treated (n = 4) or not treated (n = 4) with 55 mM KCl. The graph shows quantification for the relative protein abundance.

(B) Western blot (above) for GluR1 and GAPDH in synaptosomes from acute hippocampal slices with either control antibody (n = 5), 55 mM KCl (n = 5), or Nogo-A function-blocking antibody (n = 3) and quantification for the relative protein amount (below).

(C) mEPSC recordings before and 10 min after the application of control or Nogo-A blocking antibody. Scale bars, 20 pA and 200 ms.

(D and E) mEPSC amplitude (D) and frequency (E) percentage change upon control (black, n = 10) or Nogo-A blocking antibody (red, n = 11, ANOVA treatment, $p < 0.01$, $F_{1,19} = 14.13$).

Values represent means ± SEMs. *$p < 0.05$, ***$p < 0.001$, ****$p < 0.0001$.

inhibitory peptide (Delekate et al., 2011; Oertle et al., 2003), was used to verify the specific activity of Nogo-A on inhibitory synaptic transmission. A short application of the Δ20 peptide resulted in a rapid significant increase in mIPSC amplitude up to ~5% at 5 and 10 min after peptide application relative to the controls (Figures 1B and 1F; 5 min: $p < 0.05$; Figure S1B; Table S1) without altering the mIPSC frequency (Figures 1B, 1J, and S1E; Table S1).

To analyze the downstream signaling of Nogo-A on inhibitory synaptic transmission, loss-of-function approaches were used for two of the known Nogo-A receptors, S1PR2 and NgR1, binding the NiG-Δ20 and the Nogo-66 inhibitory domains, respectively. Application of the S1PR2 antagonist JTE-013 led to a significant decrease in mIPSC amplitude beginning at 5 and peaking at 15 min, with a reduction of ~10% relative to the control (Figures 1C and 1G; 10 min: $p < 0.01$; 15 min: $p < 0.05$; Figure S1C; Table S1), comparable to the one observed upon blocking Nogo-A. Moreover, mIPSC frequency was significantly decreased overall (Figures 1C, 1K, and S1F; Table S1). On the contrary, when a function-blocking antibody against NgR1 was used, no alterations could be observed in mIPSC amplitude (Figures 1D and 1H; Table S1) and frequency (Figures 1D and 1L; Table S1).

These results indicate that Nogo-A signaling rapidly strengthens inhibitory synaptic transmission via the S1PR2.

Activity-Dependent Localization of Nogo-A at Synapses

Next, we assessed whether the synaptic localization of Nogo-A is regulated by neuronal activity. To increase neuronal activity, acute mouse hippocampal slices were incubated with 55 mM KCl. The amount of Nogo-A in synaptosomes was decreased by ~40% upon stimulation via KCl (Figure 2A; Ctrl: 1.000 ± 0.031; KCl: 0.582 ± 0.062; $p < 0.01$), showing that the synaptic localization of Nogo-A is regulated in an activity-dependent manner. In addition, while KCl slightly increased the AMPAR subunit GluA1 in synaptosomes, Nogo-A loss of function resulted in a significant, ~2.5-fold increase in GluA1 protein levels (Figure 2B; Ctrl: 1.000 ± 0.390; KCl: 1.489 ± 0.331; Nogo-A antibody [Ab]: 2.571 ± 0.378; $p < 0.05$) confirming the role of Nogo-A in modulating excitatory synaptic transmission (Kellner et al., 2016). Acute Nogo-A loss of function led to a fast, significant increase in the amplitude of miniature excitatory postsynaptic currents (mEPSCs) peaking 10 min after antibody application, with an increase of ~15% relative to the control condition (Figures 2C and 2D; 10 min: $p < 0.001$; 15 min: $p < 0.05$; Table S1). No difference could be observed in mEPSC frequency (Figures 2C and 2E; Table S1).

The results so far indicate that upon changes in neuronal activity, Nogo-A signaling at synapses rapidly regulates inhibitory and excitatory synaptic transmission in a reciprocal manner.

Nogo-A Signaling Promotes $GABA_AR$ Clustering at Synapses via the S1PR2

As the strength of inhibitory synaptic transmission is reflected in the number of $GABA_ARs$ at synapses (Kilman et al., 2002; Nusser et al., 1997), we next tested whether Nogo-A signaling controls the localization of $GABA_ARs$. Live-labeling was used to visualize surface localization of the $GABA_AR$ γ2 subunit in mouse primary hippocampal neurons (Figures 3A–3D). A 10-min loss of function of Nogo-A, by blocking antibody application, resulted in a significant decrease in the $GABA_AR$ cluster density of ~15% (Figure 3E, $p < 0.01$; Table S2), fluorescence intensity of ~30% (Figure 3F, $p < 0.001$; Table S2), and $GABA_AR$ colocalization with synapsin$^+$ puncta of ~20% (Figure 3G, $p < 0.001$; Table S2). In contrast, a 10-min gain of function for the Nogo-A NiG-Δ20 domain, via the application of the soluble Δ20 inhibitory peptide, resulted in a significant increase in $GABA_AR$ cluster density of ~15% (Figure 3H, $p < 0.05$; Table S2) and fluorescence intensity of ~30% (Figure 3I, $p < 0.01$; Table S2). $GABA_AR$ colocalization with synapsin$^+$ puncta was slightly increased (Figure 3J; Table S2). Furthermore, a 10-min

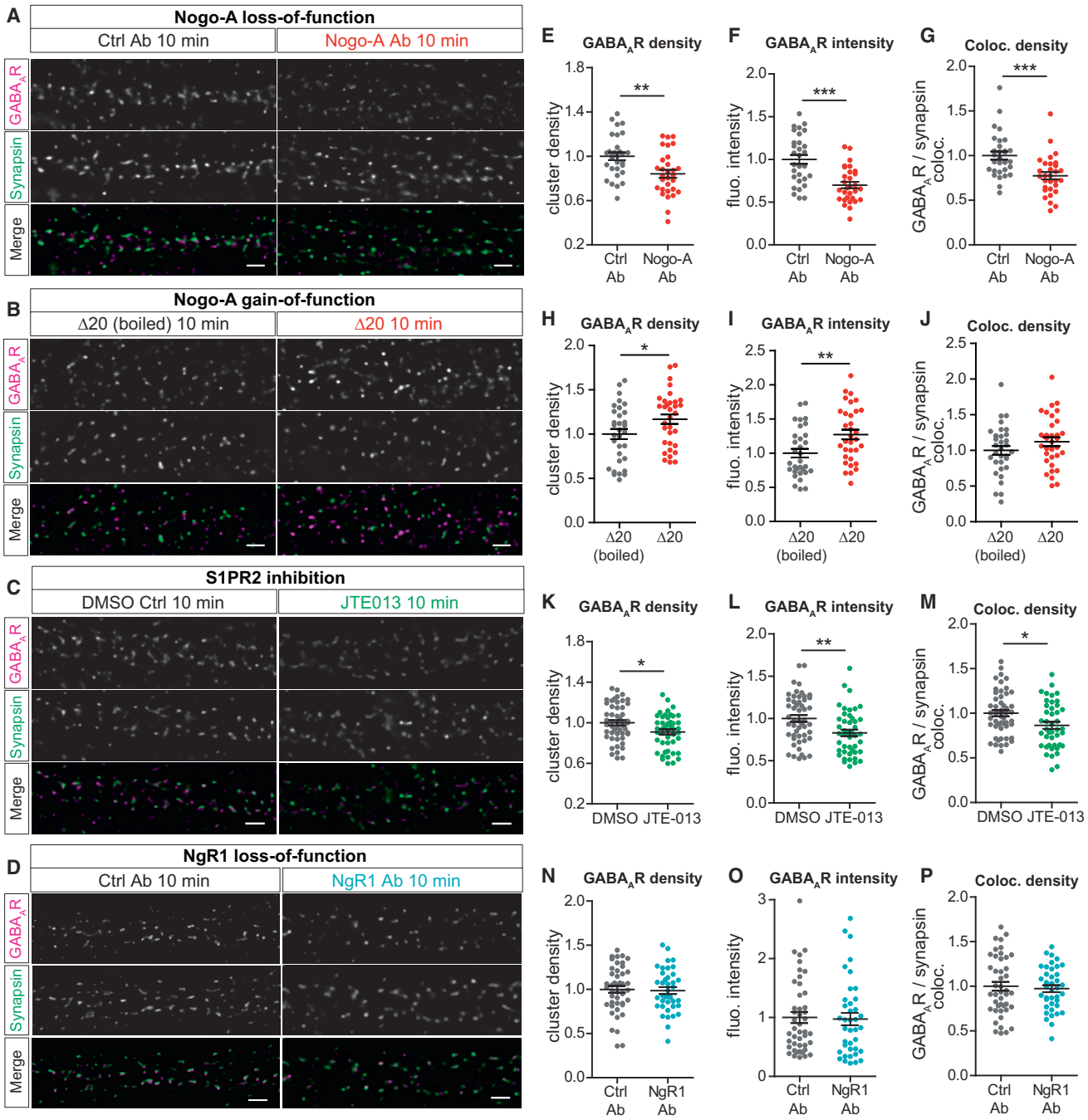

Figure 3. Nogo-A Signaling Promotes $GABA_AR$ Clustering at Synapses via the S1PR2

(A–D) Live-cell immunolabeling of surface $GABA_ARs$ followed by immunofluorescence for synapsin in primary hippocampal neurons treated for 10 min with control (A, left) or Nogo-A blocking antibody (A, right), boiled Δ20 (B, left) or Δ20 peptide (B right), DMSO (C, left) or S1PR2 inhibitor JTE-013 (C, right), and control (D, left) or NgR1 neutralizing antibody (D, right). All of the images underwent deconvolution and were equally increased in brightness and contrast by the same absolute values. Scale bar, 2 μm.

(E–P) Normalized $GABA_AR$ cluster density, fluorescence intensity, and density of colocalized $GABA_AR$ and synapsin$^+$ puncta upon Nogo-A loss of function (E–G, red, n = 30; Ctrl Ab, gray, n = 30), Nogo-A gain of function (H–J, red, n = 33; boiled Δ20 peptide, gray, n = 32), S1PR2 loss of function (K–M, green, n = 43; DMSO Ctrl, gray, n = 51), and NgR1 loss of function (N–P, blue, n = 39; Ctrl Ab, gray, n = 45).

Values represent means ± SEMs. *$p < 0.05$, **$p < 0.01$, ***$p < 0.001$.

application of the antagonist for the NiG-Δ20 specific receptor S1PR2 (JTE-013) led to a significant decrease in $GABA_AR$ cluster density of ~10% (Figure 3K, $p < 0.05$; Table S2), fluorescence intensity of ~20% (Figure 3L, $p < 0.01$; Table S2), and $GABA_AR$ colocalization with synapsin$^+$ puncta of ~15% (Figure 3M, $p < 0.05$; Table S2). On the contrary, upon both 10-min NgR1 loss of function and Nogo-66 gain of function via the NgR function-blocking antibody or the Nogo P4 peptide, no alterations were observed in $GABA_AR$ cluster density (Figures 3N and S2A; Table S2), fluorescence intensity (Figures 3O and S2B; Table S2), or $GABA_AR$ colocalization with synapsin$^+$ puncta (Figures 3P and S2A; Table S2). Under all of the experimental conditions, the density (Figures S2D–S2L; Table S3) and fluorescence intensity (Figures S2E–S2M; Table S3) of synapsin$^+$ puncta were not affected.

In summary, these findings show that the Nogo-A NiG-Δ20 domain signaling via S1PR2 positively regulates the number of $GABA_AR$ clusters and the localization of surface $GABA_ARs$ at synapses.

Nogo-A Loss of Function Increases $GABA_AR$ Diffusion Dynamics

Lateral diffusion of $GABA_ARs$ along the plasma membrane and their exchange between intra- and extrasynaptic sites contribute to the inhibitory synaptic transmission by allowing the alteration of the number of surface $GABA_ARs$ at synapses. Quantum dot-based single-particle tracking (QD-SPT; Bannai et al., 2006) was used to assess whether Nogo-A restricts inhibitory transmission by controlling $GABA_AR$ diffusion dynamics in rat primary hippocampal neurons. The application of Nogo-A blocking antibodies (Figure 4A, red; Nogo-A Ab 0 min: 1.000 ± 0.042; 10 min: 1.255 ± 0.104; $p < 0.05$) resulted in a significant increase in the membrane surface explored by QD-$GABA_AR$ diffusion over time compared to controls (Figure 4A, black; Ctrl Ab 0 min: 1.000 ± 0.058; 10 min: 0.990 ± 0.072). Accordingly, while the increase in mean square displacement (MSD) of QD-$GABA_ARs$ for cells treated with control antibodies did not change over time, in cells treated with Nogo-A blocking antibodies, it became significantly higher both at synaptic (Figures S3A and S3B; Table S4) and extrasynaptic sites (Figures S3C and S3D; Table S4). Moreover, we used the MSD of all of the trajectories at synaptic and extrasynaptic locations (see Method Details) to calculate the initial diffusion coefficient (D [$\mu m^2/s$]) of labeled $GABA_ARs$ as a measure of their local mobility. Labeled $GABA_ARs$ that had a $D < 0.004\ \mu m^2/s$ were judged immobile. Nogo-A loss of function led to a significant decrease in the $GABA_AR$ immobile fractions both at synaptic (Figure 4D; Table S4) and extrasynaptic (Figure 4E; Table S4) sites. At the same time, the size of the mobile $GABA_AR$ fractions ($D > 0.004\ \mu m^2/s$) was significantly increased at 5 and 10 min after Nogo-A blocking antibody application (Figures 4D and 4E), relative to controls (Figures 4B and 4C). While the application of the control antibody did not alter $GABA_AR$ mobility over time (Figures 4F and 4G; Table S4), Nogo-A loss of function resulted in a rapid, significant increase in the $GABA_AR$ diffusion coefficient at synaptic (Figure 4F; Table S4) and extrasynaptic (Figure 4G; Table S4) sites. The increase in the $GABA_AR$ diffusion coefficient was transient, peaking after 10 min and returning to baseline 20 min after the application of Nogo-A blocking antibody in comparison to control treated cultures (Figures 4F and 4G; Table S4). Moreover, while the mean confinement of QD-$GABA_ARs$ was not significantly changed by control antibodies, there was a significant increase in confinement upon Nogo-A loss of function (Figure S3E; Table S4).

These results indicate that Nogo-A rapidly modulates the $GABA_AR$ diffusion dynamics to promote inhibitory synaptic transmission.

Nogo-A Modulates $GABA_AR$ Clustering Independently of Gephyrin

The clustering of $GABA_ARs$ at synapses has been reported to be dependent also on the scaffold protein gephyrin confining $GABA_ARs$ at inhibitory synapses (Petrini et al., 2014; Tyagarajan and Fritschy, 2014). To test whether Nogo-A regulates gephyrin clustering, immunofluorescence for gephyrin was used in primary hippocampal neurons (Figure 5A). After 10 min of Nogo-A loss of function, the density (Figure 5B; Table S2) and fluorescence intensity (Figure 5C; Table S2) of gephyrin clusters, as well as their colocalization with synapsin$^+$ puncta, were only slightly, not significantly, reduced (Figure 5D; Table S2) compared to the control antibody treatment. No differences were observed in the density and fluorescence intensity (Figure S2O; Table S3) of synapsin$^+$ puncta (Figure S2N; Table S3).

These findings indicate that 10 min of Nogo-A loss of function do not significantly influence gephyrin clustering and suggest a mechanism by which Nogo-A may directly influence $GABA_AR$ surface dynamics independently of changes in gephyrin clustering.

Nogo-A Loss of Function Increases Ca^{2+} Dynamics in Hippocampal Neurons to Promote $GABA_AR$ Diffusion

$GABA_AR$ clustering and lateral motility are regulated by Ca^{2+} influx into neurons (Bannai et al., 2009, 2015). To assess whether Nogo-A modulates Ca^{2+} dynamics, Ca^{2+} transients were recorded over time at dendritic spines in GCaMP5g expressing mouse primary hippocampal neurons. Nogo-A loss of function resulted in a significant ~2.5-fold increase in the amplitude of Ca^{2+} transients already 10 and up to 30 min after antibody application (Figures 6A, 6B, and S5L; Tables S3 and S6; 20 min: $p < 0.05$; 30 min: $p < 0.01$) when compared to controls. On the contrary, a gain-of-function approach for the NiG-Δ20 domain of Nogo-A, via the application of the Δ20 inhibitory peptide, was found to reduce Ca^{2+} transient amplitude (Figure 6B; Table S6), compared to the control peptide. While NgR1 loss of function did not increase the amplitude of Ca^{2+} transients (Figures 6B and S5L; Tables S3 and S6), S1PR2 inhibition led to a significant increase in the amplitude of Ca^{2+} transients that returned to baseline level 30 min after JTE-013 application (Figures 6B and S5L; 10 min: $p < 0.01$; 20 min: $p < 0.05$, Tables S3 and S6) when compared to controls. No alterations could be observed in the frequency of Ca^{2+} transients under all experimental conditions (Figures 6C and S5M; Tables S3 and S6).

The results so far suggest a possible correlation between the increase in the amplitude of Ca^{2+} transients upon Nogo-A loss of function and the increase in $GABA_AR$ dynamics. To investigate the relation between the regulation of Ca^{2+} signaling and

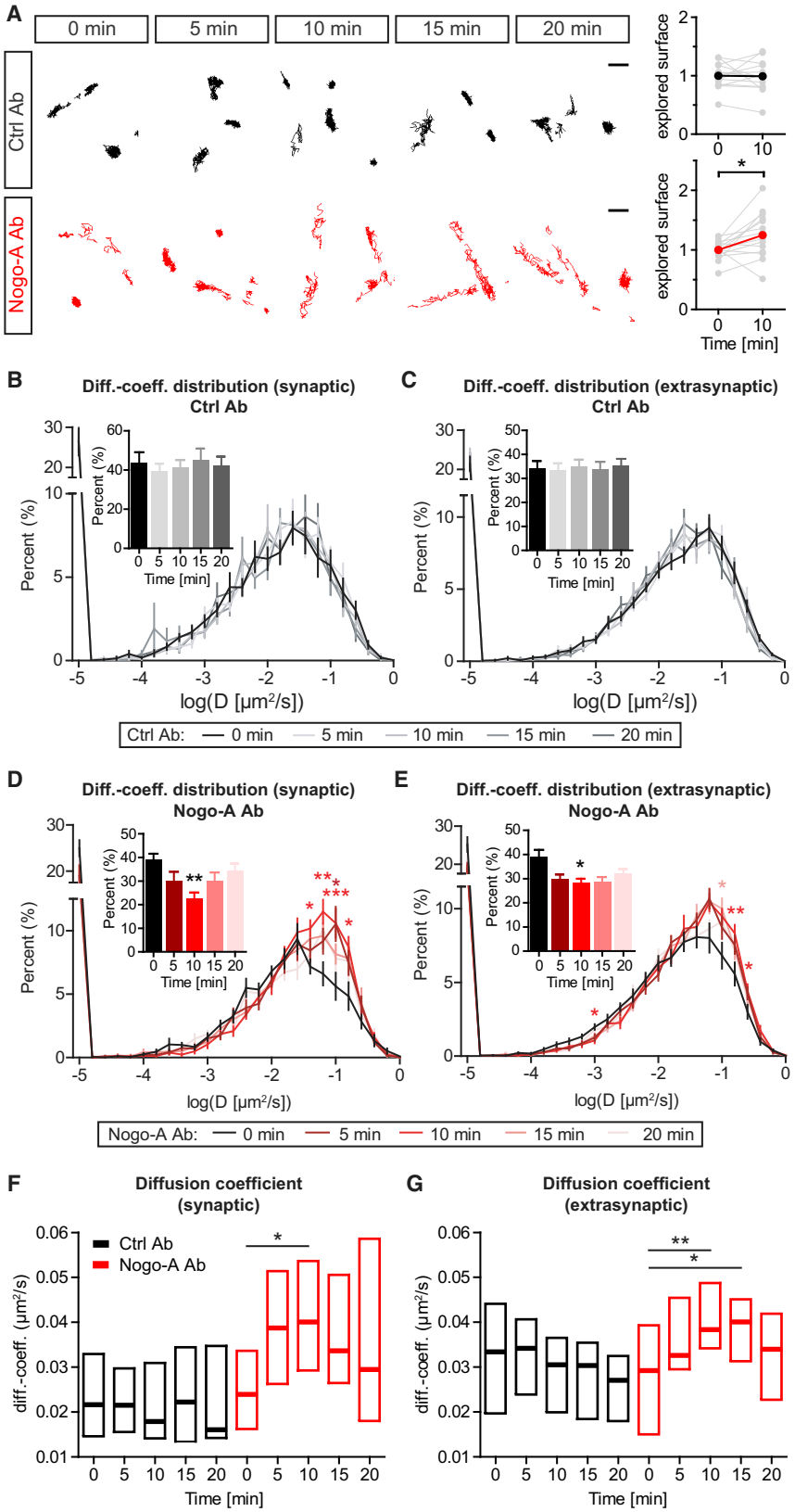

Figure 4. Nogo-A Loss of Function Increases $GABA_AR$ Diffusion Dynamics

(A) Left: trajectories of $GABA_AR$-QDs recorded for 30 s in 5-min intervals up to 20 min in primary hippocampal neurons treated with control (black) or Nogo-A blocking antibody (red). Scale bars, 2 µm. Right: average surface explored by QD-$GABA_AR$ upon control (above, black, n = 14) and Nogo-A blocking antibody (below, red, n = 14) at 0 and 10 min.

(B–E) Percentage of fractions of the logarithmic diffusion coefficient (D, diffusion coefficient) of $GABA_AR$-QDs upon treatment with control (grays) or Nogo-A blocking antibody (reds) at synaptic (B and D) and extrasynaptic sites (C and E) in 5-min intervals and up to 20 min. Bar graphs show the percentage of the immobile $GABA_AR$-QD fraction ($D < 0.004$ µm^2/s) over time (Ctrl Ab, n = 13; Nogo-A Ab, n = 14).

(F and G) Median diffusion coefficients of QD-$GABA_ARs$ with interquartile ranges (IQRs) upon control (black) or Nogo-A blocking antibody (red) at synaptic (F) and extrasynaptic sites (G). Overall, 39,137 trajectories from 14 fields of view (FOVs, 14 coverslips and 4 preparations) were analyzed in Nogo-A loss-of-function experiments (synaptic: 0 min = 2,782, 5 min = 2,664, 10 min = 2,687, 15 min = 2,253, 20 min = 1,848; extrasynaptic: 0 min = 5,582, 5 min = 5,768, 10 min = 5,703, 15 min = 5,636, 20 min = 4,214). Overall, 35,193 trajectories from 13 FOVs (13 coverslips and 4 preparations) were analyzed for the control antibody (synaptic: 0 min = 2,579, 5 min = 2,450, 10 min = 2,471, 15 min = 2,345, 20 min = 1,904; extrasynaptic: 0 min = 5,181, 5 min = 5,052, 10 min = 4465, 15 min = 4,895, 20 min = 3,851). Values represent means ± SEMs. *p < 0.05, **p < 0.01, ***p < 0.001.

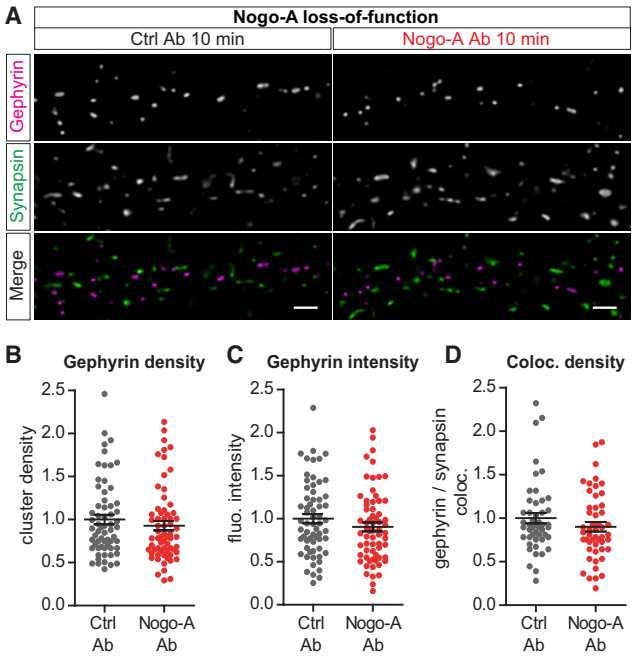

Figure 5. Nogo-A Modulates GABA$_A$R Clustering Independently of Gephyrin

(A) Immunofluorescence for gephyrin and synapsin in primary hippocampal neurons treated for 10 min with control (left) or Nogo-A blocking antibody (right). All of the images underwent deconvolution and were equally increased in brightness and contrast by the same absolute values. Scale bars, 2 μm.

(B–D) Normalized density of gephyrin clusters (B), fluorescence intensity (C), and density of gephyrin clusters colocalized with synapsin$^+$ puncta (D, Ctrl Ab, n = 48; Nogo-A Ab, n = 50) upon treatment with control (gray, n = 63) or Nogo-A blocking antibody (red, n = 65).

Values represent means ± SEMs.

GABA$_A$R diffusion dynamics at a single-cell level, QD-SPT was used to track GABA$_A$Rs in rat primary hippocampal neurons loaded with the Ca^{2+} indicator Fluo-4 AM to simultaneously visualize Ca^{2+} dynamics within the dendrites of the same neuron (Figure 6D). Again, Nogo-A loss of function resulted in an increase in the diffusion coefficient of GABA$_A$Rs at synaptic (Figure S4C; 5 and 10 min: $p < 0.01$; Table S5) and extrasynaptic sites (Figure S4D; Table S5) relative to the control conditions (Figures S4A and S4B; Table S5). Moreover, normalized GABA$_A$R diffusion dynamics were significantly increased at synaptic (Figure 6E, ~+120%; 5 min: $p < 0.01$; 10 min: $p < 0.05$; Table S5) and extrasynaptic sites (Figure 6F, ~+180%; 10 min: $p < 0.01$; Table S5) after Nogo-A loss of function compared to controls. This effect derived from a decrease in less mobile and immobile GABA$_A$R fractions ($D < 0.004$ μm^2/s) associated with an increase in the mobile fractions of GABA$_A$Rs ($D > 0.004$ μm^2/s) both at synaptic and extrasynaptic sites compared to controls (Figures S4E–S4H; Table S5). The normalized Fluo-4 fluorescence intensity (F/F_0) increased rapidly after Nogo-A blocking antibody application (Figure 6G; 5 min: 1.553 ± 0.100; 10 min: 1.768 ± 0.146; 5 min: $p < 0.05$; 10 min: $p < 0.01$) and was significantly different from the one observed in controls after both 5 and 10 min (Figure 6G; 5 min: 1.114 ± 0.081; 10 min: 1.315 ± 0.090). Also, when looking at a single-cell level, we found a positive correlation between the peak of Fluo-4 normalized fluorescence intensity and the change in diffusion dynamics in controls (Figure 6H; $R_{Spearman} = 0.429$) and significant upon Nogo-A loss of function (Figure 6H; $R_{Spearman} = 0.650$; $p < 0.05$). Finally, live-labeling for surface GABA$_A$R subunit γ2 in mouse primary hippocampal neurons was combined with the application of the Ca^{2+} chelating agent EGTA during treatment with Nogo-A blocking antibodies (Figure 6I). While, as expected, treatment with Nogo-A blocking antibodies alone significantly decreased GABA$_A$R cluster density (Figures 6I and 6J; Nogo-A Ab versus Ctrl: $p < 0.01$; Table S2), fluorescence intensity (Figure 6K; Nogo-A Ab versus Ctrl: $p < 0.05$; Table S2), and GABA$_A$R colocalization with synapsin$^+$ puncta (Figure 6L; Nogo-A Ab versus Ctrl: $p < 0.001$; Table S2), combining the Nogo-A blocking antibodies with EGTA completely prevented these effects (Figures 6J–6L). Neither the density (Figures S4I and S4J; Table S3) nor the fluorescence intensity (Figures S4I and S4K; Table S3) of synapsin$^+$ puncta were affected.

These results suggest that Nogo-A controls Ca^{2+} dynamics in hippocampal neurons to limit GABA$_A$R lateral movement, and thereby their localization at synapses.

Nogo-A Controls GABA$_A$R Localization at Synapses via the Ca^{2+}-Dependent Phosphatase Calcineurin

GABA$_A$R clustering and diffusion dynamics are regulated via changes in the activation of the Ca^{2+}-dependent protein phosphatase 3 calcineurin (CaN; Muir et al., 2010; Nakamura et al., 2015; Niwa et al., 2012). We asked whether the ability of Nogo-A signaling to promote Ca^{2+} dynamics may be involved in regulating GABA$_A$R clustering at synapses by altering CaN activity. Live-labeling for surface GABA$_A$R subunit γ2 was used in mouse primary hippocampal neurons treated with control or Nogo-A function-blocking antibodies with or without the specific CaN inhibitor cyclosporin A (Cys A; Figure 7A). A 10-min Nogo-A loss of function significantly decreased GABA$_A$R cluster density (Figure 7B, $p < 0.01$; Table S2), fluorescence intensity (Figure 7C, $p < 0.05$; Table S2) and their colocalization with synapsin$^+$ puncta (Figure 7D, $p < 0.05$; Table S2). The co-application of Cys A and the Nogo-A blocking antibody completely prevented the decrease in GABA$_A$R cluster density (Figure 7B; Table S2), fluorescence intensity (Figure 7C; Table S2), and colocalization with synapsin$^+$ puncta (Figure 7D; Table S2).

CaN regulates GABA$_A$R clustering and lateral diffusion by dephosphorylating GABA$_A$R γ2 subunit at Ser327 (Muir et al., 2010). Thus, we hypothesized that Nogo-A signaling regulates GABA$_A$R γ2 subunit phosphorylation at Ser327, thereby controlling synaptic localization of GABA$_A$Rs. Phosphorylation at Ser327 of the GABA$_A$Rs γ2 subunit was immunocytochemically detected in mouse primary hippocampal neurons treated with Nogo-A blocking or control antibodies (Figure 7E). Nogo-A loss of function for 10 min resulted in a decrease in the GABA$_A$R γ2 pSer327 density (Figure 7F; $p < 0.05$, Table S2), fluorescence intensity (Figure 7G; $p < 0.001$, Table S2), and overlap between pSer327$^+$ and GABA$_A$R$^+$ puncta (Figure 7H; $p < 0.05$, Table S2). However, co-application of the CaN inhibitor Cys A with the Nogo-A blocking antibody completely prevented the

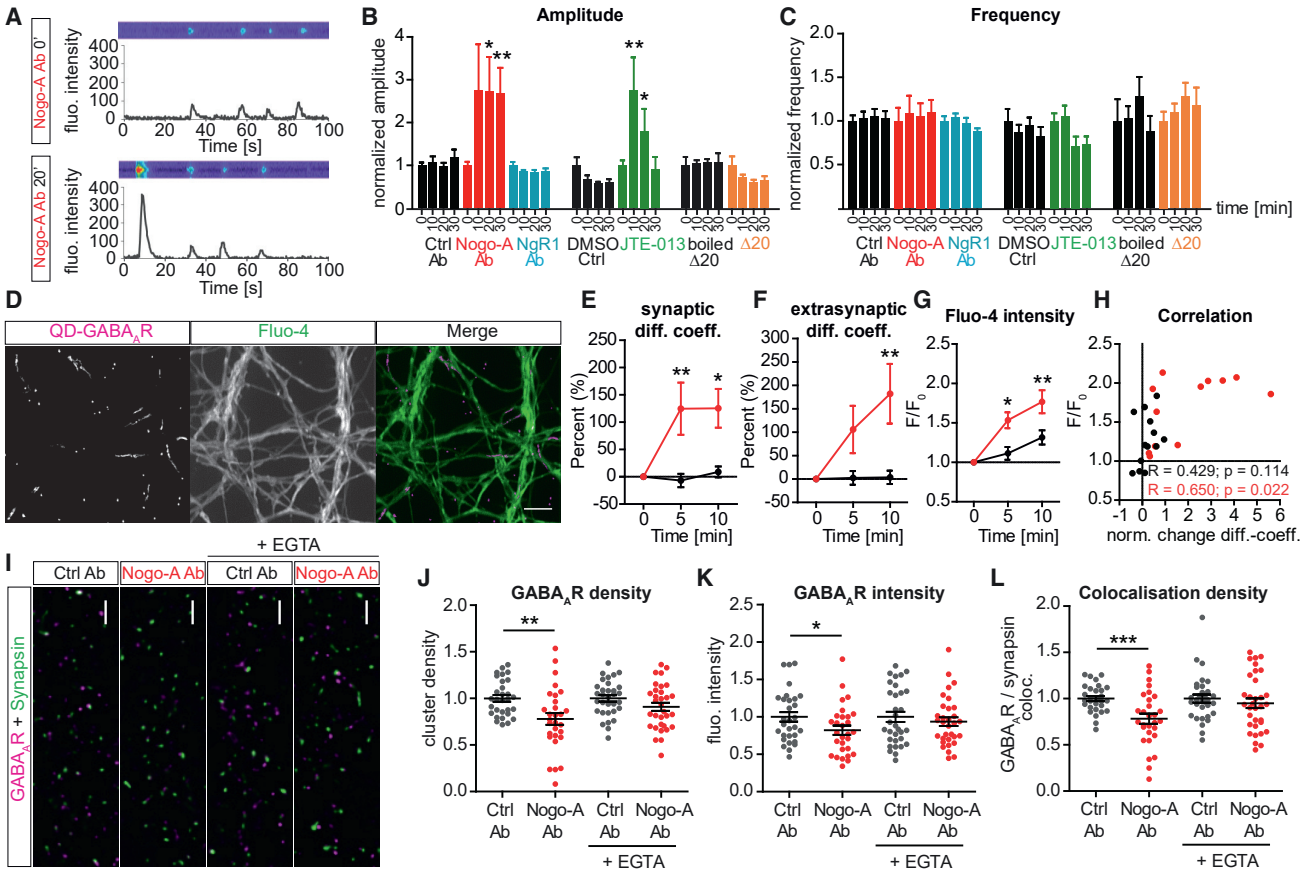

Figure 6. Nogo-A Loss of Function Increases Ca^{2+} Dynamics in Hippocampal Neurons to Promote $GABA_AR$ Diffusion

(A) Images and relative fluorescence intensity traces for GCaMP5g expressing primary hippocampal neurons before (0 min, above) and after (20 min, below) application of Nogo-A blocking antibody.

(B and C) Normalized Ca^{2+} transient amplitude (B) and frequency (C) over time for dendritic spines of primary hippocampal neurons treated with, from left, control (black, n = 42), Nogo-A blocking (red, ANOVA treatment, $p < 0.01$, $F_{1,62} = 8.014$, n = 37), NgR1 blocking antibody (blue, n = 11), control DMSO (black, n = 15), S1PR2 antagonist JTE-013 (green, ANOVA treatment, $p < 0.01$, $F_{1,28} = 8.490$, n = 15), boiled Δ20 peptide (black, n = 6), or Δ20 peptide (orange, ANOVA treatment, $p = 0.058$, $F_{1,16} = 4.318$, n = 8).

(D) $GABA_AR$-QD trajectories over 30 s and Fluo-4 fluorescence in primary hippocampal neurons. Scale bar, 5 μm.

(E and F) Normalized percentage change over time for the diffusion coefficient median upon control (black, n = 12) and Nogo-A blocking antibody (red, n = 12) at synaptic (E, ANOVA treatment, $p < 0.001$, $F_{1,24} = 16.25$) and extrasynaptic sites (F, ANOVA treatment, $p < 0.01$, $F_{1,24} = 8.006$).

(G) Normalized Fluo-4 fluorescence intensity change over time (F/F_0) for control (black, n = 12) and Nogo-A blocking antibody (red, ANOVA treatment, $p < 0.001$, $F_{1,24} = 9.804$, n = 12).

(H) Correlation between the peak value for the Fluo-4 fluorescence intensity change (F/F_0) and the diffusion coefficient for control (black dots, n = 12) and Nogo-A blocking antibody (red dots, n = 12).

(I) Hippocampal primary neurons treated with control or Nogo-A blocking antibody with or without EGTA and stained for surface $GABA_ARs$ and synapsin. All of the images underwent deconvolution and were equally increased in brightness and contrast by the same absolute values. Scale bars, 2 μm.

(J–L) Normalized $GABA_AR$ cluster density (J), fluorescence intensity (K), and colocalization of $GABA_AR$ and synapsin$^+$ puncta (L) upon Nogo-A loss of function with (Ctrl Ab, n = 32; Nogo-A Ab, n = 33) or without EGTA (Ctrl Ab, n = 30; Nogo-A Ab, n = 29).

Values represent means ± SEMs. *$p < 0.05$, **$p < 0.01$, ***$p < 0.001$.

decrease in all of the above parameters for $GABA_AR$ γ2 (Figures 7F–7H; Table S2). $GABA_AR$ γ2 puncta density (Figure S5G; Table S2) and fluorescence intensity (Figure S5H; Table S2) were not affected, indicating that the treatment did not affect the total number of $GABA_ARs$. Finally, to confirm the requirement for the $GABA_AR$ γ2 dephosphorylation at pSer327 for the regulation of $GABA_AR$ localization by Nogo-A loss of function, live-labeling of surface $GABA_AR$ subunit α2 was used for hippocampal primary neurons transfected with an myc-tagged γ2 $GABA_AR$ subunit, either with its S327 phosphorylation site intact (γ2-myc) or with S327 mutated to alanine ($\gamma2^{S327A}$-myc; Muir et al., 2010). While neurons transfected with γ2-myc showed a significant reduction in $GABA_AR$ α2 cluster intensity upon a 10-min Nogo-A loss of function (Figure 7K; $p < 0.05$, Table S2), this was completely prevented by $\gamma2^{S327A}$-myc expression (Figure 7K; Table S2). No changes could be observed in cluster density (Figure 7J; Table S2) and colocalization between $GABA_AR$ α2 and synapsin$^+$ puncta (Figure 7L; Table S2).

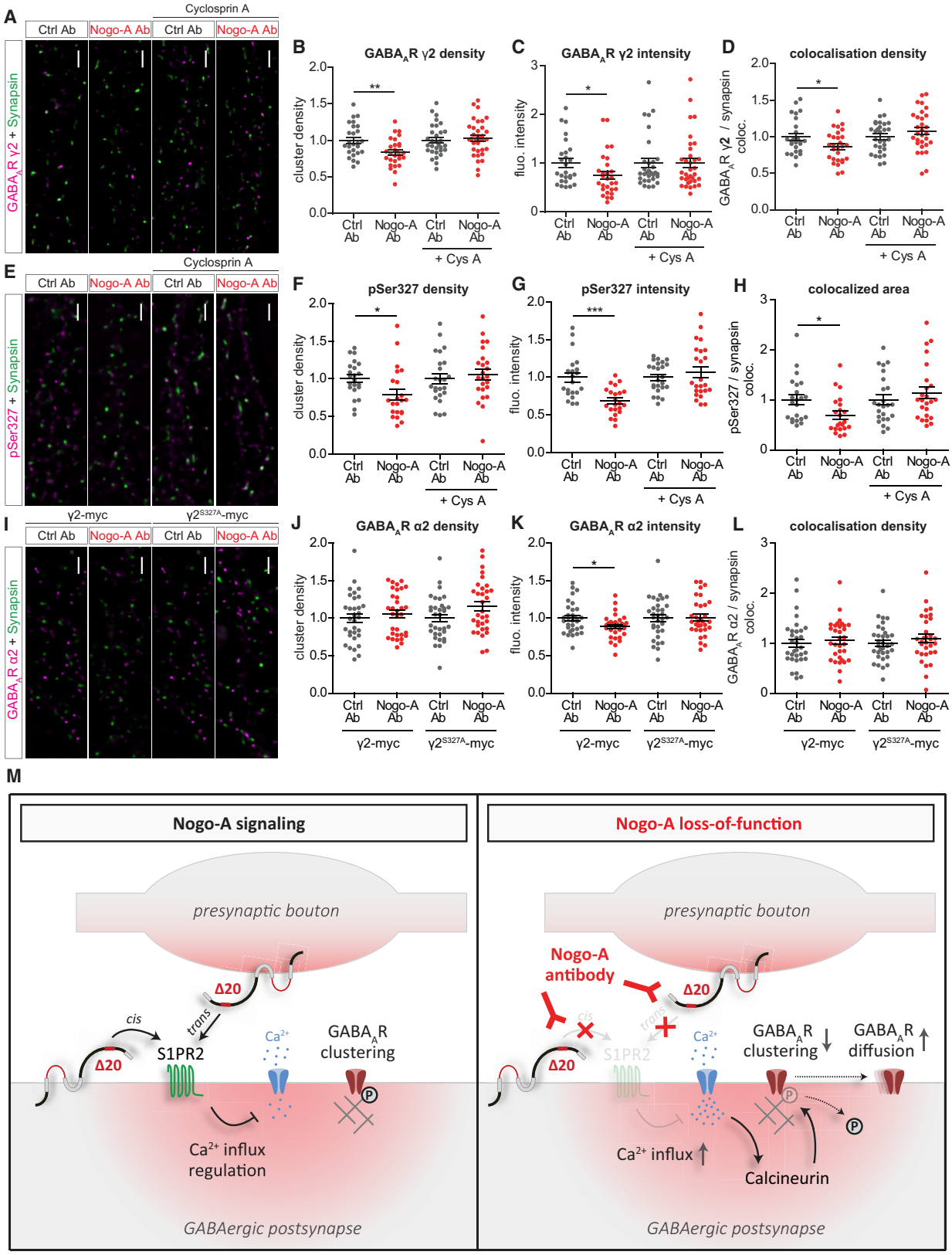

(legend on next page)

Synapsin$^+$ puncta density and fluorescence intensity (Figures S4 and S5; Table S3) were unchanged in all of the experimental conditions.

These findings indicate that a loss of function for Nogo-A signaling rapidly regulates $GABA_AR$ localization at synapses by modulating the CaN activation status, resulting in the dephosphorylation of $GABA_AR$ subunit $\gamma2$ at pSer327.

DISCUSSION

In this study, we show that Nogo-A signaling restricts inhibitory synaptic transmission by controlling the synaptic accumulation and the diffusion dynamics of $GABA_ARs$ in primary hippocampal neurons. While a gain of function for the Nogo-A NiG-Δ20 domain increases the mIPSC amplitude and the intensity of synaptic $GABA_AR$ clusters, blocking the function of this Nogo-A domain or its receptor S1PR2 results in the rapid decrease in mIPSC amplitude and in the reduced size of synaptic $GABA_AR$ clusters. These effects are due to an increase in the lateral diffusion of $GABA_ARs$ at both synaptic and extrasynaptic sites as seen using SPT of $GABA_ARs$ labeled with quantum dots. The regulation of $GABA_AR$ diffusion dynamics by Nogo-A signaling occurs at a timescale of minutes and depends upon an increase in intracellular Ca^{2+} and the activation of the phosphatase CaN.

The diffusion properties of surface $GABA_ARs$ in hippocampal neurons have been previously shown to depend on the activity-dependent increase in the intracellular Ca^{2+} concentration $[Ca^{2+}]_i$ (Bannai et al., 2009). Here, the Fluo-4 imaging shows a strong increase in $[Ca^{2+}]_i$ following Nogo-A loss of function as well as a positive correlation between the increase in $[Ca^{2+}]_i$ and in $GABA_AR$ lateral diffusion. Moreover, by co-application of EGTA, we show that the increase in Ca^{2+} dynamics upon Nogo-A loss of function is required for its effect on $GABA_AR$ localization at synapses. Our results also confirm the previously observed increase in excitatory synaptic transmission (Berry et al., 2018; Kellner et al., 2016; Figure 2) and a significant increase in the amount of AMPARs at synapses upon Nogo-A function-blocking. While an increase in $[Ca^{2+}]_i$ is associated with an increase in the diffusion coefficient of $GABA_ARs$ (Bannai et al., 2009), high $[Ca^{2+}]_i$ results in a decrease in the movement of AMPARs due to their increased confinement (Borgdorff and Choquet, 2002; Heine et al., 2008). The ability of Nogo-A to reciprocally regulate $GABA_AR$ and AMPAR localization at synapses by modulating $[Ca^{2+}]_i$ may represent a mechanism that rapidly tunes excitatory and inhibitory transmission in an activity-dependent manner. Our observation that the localization of Nogo-A at synapses is rapidly reduced upon an increase in neuronal activity supports this hypothesis.

The strength of inhibitory synaptic transmission is determined by the number of $GABA_ARs$ at synaptic sites, depending on their confinement, the rate of their insertion and removal, and their local lateral diffusion in the membrane (Choquet and Triller, 2013). In this study, we show that Nogo-A loss of function results in an increased lateral diffusion of $GABA_ARs$ both synaptically and extrasynaptically. This is due to an increase in the mobility of $GABA_ARs$ and a decrease in the fraction of immobile $GABA_ARs$, suggesting a general increase in the exchange of receptors between synaptic and extrasynaptic sites. The confinement of receptors at synapses is regulated by different mechanisms acting on either the localization of scaffold molecules or the strength of the receptor-scaffold interactions (Choquet and Triller, 2003; Triller and Choquet, 2005) or by a combination of the two (Bannai et al., 2009). While in previous studies the increase in lateral diffusion of $GABA_ARs$ has been shown to be followed by a delayed loss of their scaffold protein gephyrin (Bannai et al., 2009; Papadopoulos et al., 2007), we have observed different effects. Within the time we analyzed, no decrease in the density or intensity of gephyrin clusters occurred, in spite of the significant reduction in number and size of $GABA_AR$ clusters. Previous studies have shown that the gephyrin clustering at synapses depends on the integrity of F-actin and of microtubules (Charrier et al., 2006; Kirsch and Betz, 1995). Nogo-A loss of function has been shown to increase F-actin stability and to promote (Iobbi et al., 2017; Kellner et al., 2016) microtubule disassembly via a rho-kinase-dependent mechanism (Mimura et al., 2006), possibly preventing the loss of gephyrin. Previous observations indicate that gephyrin dispersal is not required for $GABA_AR$ declustering (Niwa et al., 2012). Our results suggest that the increase in $GABA_AR$ diffusion

Figure 7. Nogo-A Controls $GABA_AR$ Localization at Synapses via the Ca^{2+}-Dependent Phosphatase Calcineurin

(A) Immunofluorescence for surface $GABA_ARs$ and synapsin in primary hippocampal neurons treated for 10 min with control or Nogo-A blocking antibody without (left) or with (right) the CaN inhibitor cyclosporin A (Cys A).

(B–D) Normalized $GABA_AR$ cluster density (B), fluorescence intensity (C), and colocalization with synapsin$^+$ puncta (D) upon control or Nogo-A loss of function without (Ctrl Ab, n = 26; Nogo-A Ab, n = 28) or with (Ctrl Ab, n = 31; Nogo-A Ab, n = 34) Cys A.

(E) Immunofluorescence for pSer327 $\gamma2$, $GABA_AR$ $\gamma2$, and synapsin in hippocampal primary neurons treated for 10 min with control or Nogo-A blocking antibody without (left) or with (right) the CaN inhibitor Cys A.

(F–H) Normalized pSer327 $\gamma2$ cluster density (F), fluorescence intensity (G), and density of colocalized pSer327 $\gamma2$ and synapsin$^+$ puncta (H) upon control or Nogo-A loss of function without (Ctrl Ab, n = 22; Nogo-A Ab, n = 22) or with (Ctrl Ab, n = 24; Nogo-A Ab, n = 24) Cys A.

(I) Images of hippocampal primary neurons expressing the myc-tagged $GABA_AR$ $\gamma2$ subunit with the pSer327 phosphorylation site intact ($\gamma2$-myc, left) or mutated to alanine ($\gamma2^{S327A}$-myc, right), stained for the surface $GABA_AR$ $\alpha2$ subunit and synapsin and treated for 10 min with control or Nogo-A blocking antibody.

(J–L) Normalized $\alpha2$ cluster density (J), fluorescence intensity (K), and colocalization between $\alpha2$ and synapsin$^+$ puncta (L) upon control or Nogo-A loss of function ($\gamma2$-myc Ctrl Ab, n = 32 and Nogo-A Ab, n = 32; $\gamma2^{S327A}$-myc Ctrl Ab, n = 33 and Nogo-A Ab, n = 32). All of the images underwent deconvolution and were equally increased in brightness and contrast by the same absolute values. Scale bars, 2 μm.

(M) Scheme summarizing our findings. Under Nogo-A signaling conditions, the phosphorylation of $GABA_ARs$ at pSer327 keeps them clustered at inhibitory synapses (left). Upon Nogo-A loss of function, the influx of Ca^{2+} activates CaN, resulting in the dephosphorylation of $GABA_ARs$ at pSer327 and an increase in their lateral diffusion.

Values represent means ± SEMs. *$p < 0.05$, **$p < 0.01$, ***$p < 0.001$.

follows a change in the binding of $GABA_AR$s to the scaffold proteins rather than a declustering of gephyrin. A major mechanism regulating the trafficking of $GABA_AR$s is the direct phosphorylation and dephosphorylation of residues within the intracellular loop (Kittler and Moss, 2003; Vithlani et al., 2011). Mice in which the phosphorylation of the γ2 subunits of $GABA_AR$s is prevented show an accumulation of $GABA_AR$s at inhibitory synapses in CA3 neurons due to their aberrant trafficking (Tretter et al., 2009). In particular, a crucial role in regulating $GABA_AR$ lateral mobility is exerted by the phosphorylation status of Ser327 of the γ2 subunit, a known substrate for the Ca^{2+}-dependent phosphatase CaN (Muir et al., 2010; Wang et al., 2003). A function of CaN downstream of Nogo-A signaling in regulating the synaptic localization of $GABA_AR$s is supported by our observation that the effects of a loss-of-function approach for Nogo-A are completely prevented by the co-application of Cys A, a specific CaN inhibitor. Moreover, we observe that the phosphorylation at Ser327 of the γ2 subunit is reduced upon blocking Nogo-A, but not when the activation of CaN is prevented by co-application of Cys A. CaN has been identified as a major regulator of bidirectional plasticity due to its ability to regulate both inhibitory and excitatory synaptic transmission. While CaN also dephosphorylates AMPARs at Ser845, thereby promoting their internalization (Kessels and Malinow, 2009; Man et al., 2007), our results show a strengthening rather than a weakening of excitatory synaptic transmission and an increase in AMPARs at synapses. However, the trafficking of surface AMPARs also depends on the stability of F-actin within spines. It is conceivable that the increased F-actin stability upon Nogo-A loss of function (Kellner et al., 2016) may promote the accumulation of AMPARs at synaptic sites observed in our study. Furthermore, the studies showing a negative effect of CaN activity on the strength of excitatory synapses and long-term potentiation (LTP) rely on its genetic manipulation (Malleret et al., 2001; Sanderson et al., 2018) and therefore address much longer time points of CaN loss of function than in our experiment upon its acute inhibition via Cys A. Timing and the cellular localization and activation kinetics of CaN may influence the net outcome of its loss of function (Li et al., 2012).

We show that acute loss of function for the Nogo-A specific NiG-Δ20 inhibitory domain increases Ca^{2+} influx and strengthens excitatory synaptic transmission while reducing inhibitory synaptic transmission. These observations are consistent with recent studies showing that the blockade of Nogo-A increases functional and structural plasticity in the hippocampus and cerebral cortex (Akbik et al., 2013; Delekate et al., 2011; Jitsuki et al., 2016; Kellner et al., 2016; Lee et al., 2008; Raiker et al., 2010; Zemmar et al., 2014) and further support novel roles for this protein beyond its function as an inhibitor of neuronal regeneration upon injury (Schwab and Strittmatter, 2014). Our results in particular identify the ability of Nogo-A to modulate inhibitory synaptic transmission as a possible mechanism that mediates its role as a molecular brake acting to restrict synaptic plasticity. While a decrease in the ratio between excitation and inhibition (E/I balance) coincides with the closure of the critical period (Morales et al., 2002) and restricts plasticity to the adult levels (Levelt and Hübener, 2012; Morishita and Hensch, 2008), disinhibition initiates plasticity in the visual cortex (Kuhlman et al., 2013). Nogo-A/B and NgR1 knockout mice retain levels of plasticity that are typical of the critical period also as adults (McGee et al., 2005) and show lower levels of cortical inhibition (Stephany et al., 2014), suggesting that signaling via NgR1 limits disinhibition to drive the closure of the critical period in the visual cortex. In our study, while blocking the S1PR2 (specific receptor for the Nogo-A NiG-Δ20 domain) reproduced the increase in Ca^{2+} influx and the reduction in inhibitory synaptic transmission, a loss of function for NgR1 did not influence these parameters. However, NgR1 loss of function was shown to increase LTP (Delekate et al., 2011; Zemmar et al., 2014) and to restrict the insertion of AMPARs at synapses upon learning (Jitsuki et al., 2016). Finally, the lower inhibition levels in the visual cortex of NgR1 knockout mice have been shown to derive from a reduction in the excitatory drive onto parvalbumin$^+$ interneurons (Stephany et al., 2014), suggesting that NgR1 signaling may specifically affect excitatory and not inhibitory synaptic transmission. However, the results of experiments in which GABAergic transmission was blocked during neutralization of the Nogo-A NiG-Δ20 domain indicate that the increase in LTP following a Nogo-A loss of function may be due to the suppression of inhibition (Delekate et al., 2011). During the onset of LTP, the concomitant decrease in IPSPs is required to increase the ability of EPSPs to generate a spike (Lu et al., 2000; Wang and Stelzer, 1996). In our study, the reduction in the amplitude of mIPSCs after Nogo-A neutralization shortly precedes the increase in mEPSC amplitude. Therefore, our results suggest that, while signaling of Nogo-A or other ligands via NgR1 regulate selectively excitatory synaptic transmission, Nogo-A signaling via its S1PR2 exerts a Nogo-A-specific effect in controlling inhibitory synaptic transmission, by regulating $GABA_AR$ localization at inhibitory synapses, and their diffusion dynamics and excitatory synaptic transmission, by regulating AMPAR surface insertion. Our observation of an increase in amplitude but not in frequency of mEPSCs upon Nogo-A loss of function and the lack of loss in synapsin under this condition supports a previously suggested postsynaptic action of Nogo-A (Delekate et al., 2011). Although our current data do not support it, an involvement of the PirB receptor in modulating $GABA_AR$ dynamics can at this point not be excluded.

To consider Nogo-A as a main player in orchestrating the control of synaptic strength and in modulating the excitation-inhibition balance, its synaptic localization or the one of its receptors must be regulated by neuronal activity. We show that the surface expression of Nogo-A at synapses is reduced upon an increase in neuronal activity. While this observation leaves open the possibility that the localization of the Nogo-A receptors is also modulated by neuronal activity, it furthers our understanding about how Nogo-A can respond to changes in neuronal activity by rapidly regulating synaptic plasticity.

While the correct balance between excitation and inhibition is crucial for normal brain function, the molecular mechanisms underlying it are still largely unclear. Only recently has cadherin-10 been described as a reciprocal modulator of excitatory and inhibitory synaptic transmission by promoting excitation while suppressing inhibition (Smith et al., 2017). Moreover, while molecules that negatively modulate inhibition have been already described, for example, BDNF (Brünig et al., 2001; Goodkin

et al., 2005), less is known about molecules promoting it. We now identify Nogo-A as a reciprocal modulator of excitation and inhibition acting to simultaneously promote inhibitory and suppress excitatory synaptic transmission in the hippocampus. The signaling of Nogo-A, which is localized in an activity-dependent manner at synaptic sites in the hippocampus, rapidly increases GABAergic transmission by regulating the diffusion dynamics of $GABA_ARs$ in a $[Ca^{2+}]_i$- and CaN-dependent manner. Along with the observation that Nogo-A signaling suppresses excitatory synaptic transmission, our results support a role for Nogo-A in fine-tuning neuronal plasticity by controlling the ratio between excitation and inhibition. Understanding this contributes to the knowledge of the basic physiological homeostatic molecular mechanisms involved in controlling neuronal plasticity, and thereby learning and memory processes.

STAR★METHODS

Detailed methods are provided in the online version of this paper and include the following:

- KEY RESOURCES TABLE
- LEAD CONTACT AND MATERIALS AVAILABILITY
- EXPERIMENTAL MODEL AND SUBJECT DETAILS
  - Mice
  - Primary mouse hippocampal culture
  - Primary rat hippocampal culture
  - Mouse organotypic hippocampal slice culture
  - Acute mouse hippocampal slices
- METHOD DETAILS
  - Antibody and peptide treatment
  - Patch clamp electrophysiology
  - Transfection of primary hippocampal neurons
  - Live-cell labeling and immunofluorescence
  - Widefield fluorescence imaging and analysis
  - Single particle tracking and Fluo-4 imaging
  - Ca^{2+}-imaging
  - Synaptosome isolation
  - Western blot analysis
- DATA AND CODE AVAILABILITY

SUPPLEMENTAL INFORMATION

Supplemental Information can be found online at https://doi.org/10.1016/j.celrep.2019.09.015.

ACKNOWLEDGMENTS

We thank Martin E. Schwab (Swiss Federal Institute of Technology Zurich [ETH] and University of Zurich) for providing the Nogo-A blocking antibody, Josef Kittler (University College London) for the constructs to express the myc-tagged γ2 subunit of $GABA_ARs$, and Diane Mundil and Anita Heine for the outstanding technical assistance. The work was supported by the Deutsche Forschungsgemeinschaft to M.Z. (ZA 554/3-2) and M.K. (KO 1674/15-2).

AUTHOR CONTRIBUTIONS

S.F., K.M., M.H., M.K., and M.Z. conceptualized the study; M.K. and M.Z. acquired the funding; S.F., K.M., M.O., and S.H. performed the experiments; S.F., K.M., and M.O. performed the formal analysis of the data; M.H. provided the resources; S.F. and M.Z. wrote the original draft; M.H., M.K., S.F., and M.Z. reviewed and edited the paper.

DECLARATION OF INTERESTS

The authors declare no competing interests.

Received: March 18, 2019
Revised: July 2, 2019
Accepted: September 6, 2019
Published: October 15, 2019

REFERENCES

Akbik, F.V., Bhagat, S.M., Patel, P.R., Cafferty, W.B., and Strittmatter, S.M. (2013). Anatomical plasticity of adult brain is titrated by Nogo Receptor 1. Neuron *77*, 859–866.

Akerboom, J., Chen, T.W., Wardill, T.J., Tian, L., Marvin, J.S., Mutlu, S., Calderón, N.C., Esposti, F., Borghuis, B.G., Sun, X.R., et al. (2012). Optimization of GCaMP calcium indicator for neural activity imaging. J. Neurosci. *32*, 13819–13840.

Banker, G.A. (1980). Trophic interactions between astroglial cells and hippocampal neurons in culture. Science *209*, 809–810.

Bannai, H., Lévi, S., Schweizer, C., Dahan, M., and Triller, A. (2006). Imaging the lateral diffusion of membrane molecules with quantum dots. Nat. Protoc. *1*, 2628–2634.

Bannai, H., Lévi, S., Schweizer, C., Inoue, T., Launey, T., Racine, V., Sibarita, J.B., Mikoshiba, K., and Triller, A. (2009). Activity-dependent tuning of inhibitory neurotransmission based on GABAAR diffusion dynamics. Neuron *62*, 670–682.

Bannai, H., Niwa, F., Sherwood, M.W., Shrivastava, A.N., Arizono, M., Miyamoto, A., Sugiura, K., Lévi, S., Triller, A., and Mikoshiba, K. (2015). Bidirectional Control of Synaptic GABAAR Clustering by Glutamate and Calcium. Cell Rep. *13*, 2768–2780.

Barron, H.C., Vogels, T.P., Behrens, T.E., and Ramaswami, M. (2017). Inhibitory engrams in perception and memory. Proc. Natl. Acad. Sci. USA *114*, 6666–6674.

Berry, S., Weinmann, O., Fritz, A.K., Rust, R., Wolfer, D., Schwab, M.E., Gerber, U., and Ster, J. (2018). Loss of Nogo-A, encoded by the schizophrenia risk gene Rtn4, reduces mGlu3 expression and causes hyperexcitability in hippocampal CA3 circuits. PLoS One *13*, e0200896.

Borgdorff, A.J., and Choquet, D. (2002). Regulation of AMPA receptor lateral movements. Nature *417*, 649–653.

Brünig, I., Penschuck, S., Berninger, B., Benson, J., and Fritschy, J.M. (2001). BDNF reduces miniature inhibitory postsynaptic currents by rapid downregulation of GABA(A) receptor surface expression. Eur. J. Neurosci. *13*, 1320–1328.

Caroni, P., Savio, T., and Schwab, M.E. (1988). Central nervous system regeneration: oligodendrocytes and myelin as non-permissive substrates for neurite growth. Prog. Brain Res. *78*, 363–370.

Charrier, C., Ehrensperger, M.V., Dahan, M., Lévi, S., and Triller, A. (2006). Cytoskeleton regulation of glycine receptor number at synapses and diffusion in the plasma membrane. J. Neurosci. *26*, 8502–8511.

Chen, M.S., Huber, A.B., van der Haar, M.E., Frank, M., Schnell, L., Spillmann, A.A., Christ, F., and Schwab, M.E. (2000). Nogo-A is a myelin-associated neurite outgrowth inhibitor and an antigen for monoclonal antibody IN-1. Nature *403*, 434–439.

Choquet, D., and Triller, A. (2003). The role of receptor diffusion in the organization of the postsynaptic membrane. Nat. Rev. Neurosci. *4*, 251–265.

Choquet, D., and Triller, A. (2013). The dynamic synapse. Neuron *80*, 691–703.

Danielson, E., and Lee, S.H. (2014). SynPAnal: software for rapid quantification of the density and intensity of protein puncta from fluorescence microscopy images of neurons. Plos One *10*, e0118657.

Delekate, A., Zagrebelsky, M., Kramer, S., Schwab, M.E., and Korte, M. (2011). NogoA restricts synaptic plasticity in the adult hippocampus on a fast time scale. Proc. Natl. Acad. Sci. USA *108*, 2569–2574.

Fournier, A.E., GrandPre, T., and Strittmatter, S.M. (2001). Identification of a receptor mediating Nogo-66 inhibition of axonal regeneration. Nature *409*, 341–346.

Frischknecht, R., Fejtova, A., Viesti, M., Stephan, A., and Sonderegger, P. (2008). Activity-induced synaptic capture and exocytosis of the neuronal serine protease neurotrypsin. J Neurosci. *28*, 1568–1579.

Goodkin, H.P., Yeh, J.L., and Kapur, J. (2005). Status epilepticus increases the intracellular accumulation of GABAA receptors. J. Neurosci. *25*, 5511–5520.

GrandPré, T., Li, S., and Strittmatter, S.M. (2002). Nogo-66 receptor antagonist peptide promotes axonal regeneration. Nature *417*, 547–551.

Heine, M., Groc, L., Frischknecht, R., Béïque, J.C., Lounis, B., Rumbaugh, G., Huganir, R.L., Cognet, L., and Choquet, D. (2008). Surface mobility of postsynaptic AMPARs tunes synaptic transmission. Science *320*, 201–205.

Huber, A.B., Weinmann, O., Brösamle, C., Oertle, T., and Schwab, M.E. (2002). Patterns of Nogo mRNA and protein expression in the developing and adult rat and after CNS lesions. J. Neurosci. *22*, 3553–3567.

Iobbi, C., Korte, M., and Zagrebelsky, M. (2017). Nogo-66 Restricts Synaptic Strengthening via Lingo1 and the ROCK2-Cofilin Pathway to Control Actin Dynamics. Cereb. Cortex *27*, 2779–2792.

Isaacson, J.S., and Scanziani, M. (2011). How inhibition shapes cortical activity. Neuron *72*, 231–243.

Izeddin, I., Boulanger, J., Racine, V., Specht, C.G., Kechkar, A., Nair, D., Triller, A., Choquet, D., Dahan, M., and Sibarita, J.B. (2012). Wavelet analysis for single molecule localization microscopy. Opt Express *20*, 2081–2095.

Jitsuki, S., Nakajima, W., Takemoto, K., Sano, A., Tada, H., Takahashi-Jitsuki, A., and Takahashi, T. (2016). Nogo Receptor Signaling Restricts Adult Neural Plasticity by Limiting Synaptic AMPA Receptor Delivery. Cereb. Cortex *26*, 427–439.

Josephson, A., Widenfalk, J., Widmer, H.W., Olson, L., and Spenger, C. (2001). NOGO mRNA expression in adult and fetal human and rat nervous tissue and in weight drop injury. Exp. Neurol. *169*, 319–328.

Karlsson, T.E., Smedfors, G., Brodin, A.T., Aberg, E., Mattsson, A., Hogbeck, I., Wellfelt, K., Josephson, A., Brene, S., and Olson, L. (2016). NgR1: A Tunable Sensor Regulating Memory Formation, Synaptic, and Dendritic Plasticity. Cereb. Cortex *26*, 1804–1817.

Kellner, Y., Godecke, N., Dierkes, T., Thieme, N., Zagrebelsky, M., and Korte, M. (2014). The BDNF effects on dendritic spines of mature hippocampal neurons depend on neuronal activity. Front Synaptic Neurosci. *6*, 5.

Kellner, Y., Fricke, S., Kramer, S., Iobbi, C., Wierenga, C.J., Schwab, M.E., Korte, M., and Zagrebelsky, M. (2016). Nogo-A controls structural plasticity at dendritic spines by rapidly modulating actin dynamics. Hippocampus *26*, 816–831.

Kempf, A., Tews, B., Arzt, M.E., Weinmann, O., Obermair, F.J., Pernet, V., Zagrebelsky, M., Delekate, A., Iobbi, C., Zemmar, A., et al. (2014). The sphingolipid receptor S1PR2 is a receptor for Nogo-a repressing synaptic plasticity. PLoS Biol. *12*, e1001763.

Kessels, H.W., and Malinow, R. (2009). Synaptic AMPA receptor plasticity and behavior. Neuron *61*, 340–350.

Kilman, V., van Rossum, M.C., and Turrigiano, G.G. (2002). Activity deprivation reduces miniature IPSC amplitude by decreasing the number of postsynaptic GABA(A) receptors clustered at neocortical synapses. J. Neurosci. *22*, 1328–1337.

Kirsch, J., and Betz, H. (1995). The postsynaptic localization of the glycine receptor-associated protein gephyrin is regulated by the cytoskeleton. J. Neurosci. *15*, 4148–4156.

Kittler, J.T., and Moss, S.J. (2003). Modulation of GABAA receptor activity by phosphorylation and receptor trafficking: implications for the efficacy of synaptic inhibition. Curr. Opin. Neurobiol. *13*, 341–347.

Kuhlman, S.J., Olivas, N.D., Tring, E., Ikrar, T., Xu, X., and Trachtenberg, J.T. (2013). A disinhibitory microcircuit initiates critical-period plasticity in the visual cortex. Nature *501*, 543–546.

Kusumi, A., Sako, Y., and Yamamoto, M. (1993). Confined lateral diffusion of membrane receptors as studied by single particle tracking (nanovid microscopy). Effects of calcium-induced differentiation in cultured epithelial cells. Biophys. J. *65*, 2021–2040.

Lee, H., Raiker, S.J., Venkatesh, K., Geary, R., Robak, L.A., Zhang, Y., Yeh, H.H., Shrager, P., and Giger, R.J. (2008). Synaptic function for the Nogo-66 receptor NgR1: regulation of dendritic spine morphology and activity-dependent synaptic strength. J. Neurosci. *28*, 2753–2765.

Levelt, C.N., and Hübener, M. (2012). Critical-period plasticity in the visual cortex. Annu. Rev. Neurosci. *35*, 309–330.

Li, L., Stefan, M.I., and Le Novère, N. (2012). Calcium input frequency, duration and amplitude differentially modulate the relative activation of calcineurin and CaMKII. PLoS One *7*, e43810.

Liebscher, T., Schnell, L., Schnell, D., Scholl, J., Schneider, R., Gullo, M., Fouad, K., Mir, A., Rausch, M., Kindler, D., et al. (2005). Nogo-A antibody improves regeneration and locomotion of spinal cord-injured rats. Ann Neurol. *58*, 706–719.

Liu, Y.Y., Jin, W.L., Liu, H.L., and Ju, G. (2003). Electron microscopic localization of Nogo-A at the postsynaptic active zone of the rat. Neurosci. Lett. *346*, 153–156.

Lu, Y.M., Mansuy, I.M., Kandel, E.R., and Roder, J. (2000). Calcineurin-mediated LTD of GABAergic inhibition underlies the increased excitability of CA1 neurons associated with LTP. Neuron *26*, 197–205.

Luscher, B., Fuchs, T., and Kilpatrick, C.L. (2011). GABAA receptor trafficking-mediated plasticity of inhibitory synapses. Neuron *70*, 385–409.

Maffei, A. (2011). The many forms and functions of long term plasticity at GABAergic synapses. Neural Plast. *2011*, 254724.

Malleret, G., Haditsch, U., Genoux, D., Jones, M.W., Bliss, T.V., Vanhoose, A.M., Weitlauf, C., Kandel, E.R., Winder, D.G., and Mansuy, I.M. (2001). Inducible and reversible enhancement of learning, memory, and long-term potentiation by genetic inhibition of calcineurin. Cell *104*, 675–686.

Man, H.Y., Sekine-Aizawa, Y., and Huganir, R.L. (2007). Regulation of alpha-amino-3-hydroxy-5-methyl-4-isoxazolepropionic acid receptor trafficking through PKA phosphorylation of the Glu receptor 1 subunit. Proc. Natl. Acad. Sci. USA *104*, 3579–3584.

McGee, A.W., Yang, Y., Fischer, Q.S., Daw, N.W., and Strittmatter, S.M. (2005). Experience-driven plasticity of visual cortex limited by myelin and Nogo receptor. Science *309*, 2222–2226.

Michaelsen-Preusse, K., Kellner, Y., Korte, M., and Zagrebelsky, M. (2014). Analysis of Actin Turnover and Spine Dynamics in Hippocampal Slice Cultures. In Laser Scanning Microscopy and Quantitative Image Analysis of Neuronal Tissue, L. Bakota and R. Brandt, eds. (Humana Press), Neuromethods.

Mimura, F., Yamagishi, S., Arimura, N., Fujitani, M., Kubo, T., Kaibuchi, K., and Yamashita, T. (2006). Myelin-associated glycoprotein inhibits microtubule assembly by a Rho-kinase-dependent mechanism. J. Biol. Chem. *281*, 15970–15979.

Morales, B., Choi, S.Y., and Kirkwood, A. (2002). Dark rearing alters the development of GABAergic transmission in visual cortex. J. Neurosci. *22*, 8084–8090.

Morishita, H., and Hensch, T.K. (2008). Critical period revisited: impact on vision. Curr. Opin. Neurobiol. *18*, 101–107.

Moss, S.J., and Smart, T.G. (2001). Constructing inhibitory synapses. Nat. Rev. Neurosci. *2*, 240–250.

Muir, J., Arancibia-Carcamo, I.L., MacAskill, A.F., Smith, K.R., Griffin, L.D., and Kittler, J.T. (2010). NMDA receptors regulate GABAA receptor lateral mobility and clustering at inhibitory synapses through serine 327 on the γ2 subunit. Proc. Natl. Acad. Sci. USA *107*, 16679–16684.

Nakamura, Y., Darnieder, L.M., Deeb, T.Z., and Moss, S.J. (2015). Regulation of GABAARs by phosphorylation. Adv. Pharmacol. *72*, 97–146.

Niwa, F., Bannai, H., Arizono, M., Fukatsu, K., Triller, A., and Mikoshiba, K. (2012). Gephyrin-independent GABA(A)R mobility and clustering during plasticity. PLoS One *7*, e36148.

Nusser, Z., Cull-Candy, S., and Farrant, M. (1997). Differences in synaptic GABA(A) receptor number underlie variation in GABA mini amplitude. Neuron *19*, 697–709.

Oertle, T., van der Haar, M.E., Bandtlow, C.E., Robeva, A., Burfeind, P., Buss, A., Huber, A.B., Simonen, M., Schnell, L., Brösamle, C., et al. (2003). Nogo-A inhibits neurite outgrowth and cell spreading with three discrete regions. J. Neurosci. *23*, 5393–5406.

Papadopoulos, T., Korte, M., Eulenburg, V., Kubota, H., Retiounskaia, M., Harvey, R.J., Harvey, K., O'Sullivan, G.A., Laube, B., Hülsmann, S., et al. (2007). Impaired GABAergic transmission and altered hippocampal synaptic plasticity in collybistin-deficient mice. EMBO J. *26*, 3888–3899.

Petrini, E.M., Ravasenga, T., Hausrat, T.J., Iurilli, G., Olcese, U., Racine, V., Sibarita, J.B., Jacob, T.C., Moss, S.J., Benfenati, F., et al. (2014). Synaptic recruitment of gephyrin regulates surface GABAA receptor dynamics for the expression of inhibitory LTP. Nat. Commun. *5*, 3921.

Raiker, S.J., Lee, H., Baldwin, K.T., Duan, Y., Shrager, P., and Giger, R.J. (2010). Oligodendrocyte-myelin glycoprotein and Nogo negatively regulate activity-dependent synaptic plasticity. J. Neurosci. *30*, 12432–12445.

Sanderson, J.L., Scott, J.D., and Dell'Acqua, M.L. (2018). Control of Homeostatic Synaptic Plasticity by AKAP-Anchored Kinase and Phosphatase Regulation of Ca^{2+}-Permeable AMPA Receptors. J. Neurosci. *38*, 2863–2876.

Schnell, L., and Schwab, M.E. (1990). Axonal regeneration in the rat spinal cord produced by an antibody against myelin-associated neurite growth inhibitors. Nature *343*, 269–272.

Schwab, M.E., and Strittmatter, S.M. (2014). Nogo limits neural plasticity and recovery from injury. Curr. Opin. Neurobiol. *27*, 53–60.

Smith, K.R., Jones, K.A., Kopeikina, K.J., Burette, A.C., Copits, B.A., Yoon, S., Forrest, M.P., Fawcett-Patel, J.M., Hanley, J.G., Weinberg, R.J., et al. (2017). Cadherin-10 Maintains Excitatory/Inhibitory Ratio through Interactions with Synaptic Proteins. J. Neurosci. *37*, 11127–11139.

Stephany, C.E., Chan, L.L., Parivash, S.N., Dorton, H.M., Piechowicz, M., Qiu, S., and McGee, A.W. (2014). Plasticity of binocularity and visual acuity are differentially limited by nogo receptor. J. Neurosci. *34*, 11631–11640.

Stoppini, L., Buchs, P.A., and Muller, D. (1991). A simple method for organotypic cultures of nervous tissue. J Neurosci Methods *37*, 173–182.

Suresh, A., and Dunaevsky, A. (2015). Preparation of Synaptosomes from the Motor Cortex of Motor Skill Trained Mice. Bio Protoc. *5*, e1398.

Syken, J., Grandpre, T., Kanold, P.O., and Shatz, C.J. (2006). PirB restricts ocular-dominance plasticity in visual cortex. Science *313*, 1795–1800.

Tretter, V., Revilla-Sanchez, R., Houston, C., Terunuma, M., Havekes, R., Florian, C., Jurd, R., Vithlani, M., Michels, G., Couve, A., et al. (2009). Deficits in spatial memory correlate with modified gamma-aminobutyric acid type A receptor tyrosine phosphorylation in the hippocampus. Proc. Natl. Acad. Sci. USA *106*, 20039–20044.

Triller, A., and Choquet, D. (2005). Surface trafficking of receptors between synaptic and extrasynaptic membranes: and yet they do move!. Trends Neurosci. *28*, 133–139.

Tyagarajan, S.K., and Fritschy, J.M. (2014). Gephyrin: a master regulator of neuronal function? Nat. Rev. Neurosci. *15*, 141–156.

Vithlani, M., Terunuma, M., and Moss, S.J. (2011). The dynamic modulation of GABA(A) receptor trafficking and its role in regulating the plasticity of inhibitory synapses. Physiol. Rev. *91*, 1009–1022.

Wang, J.H., and Stelzer, A. (1996). Shared calcium signaling pathways in the induction of long-term potentiation and synaptic disinhibition in CA1 pyramidal cell dendrites. J. Neurophysiol. *75*, 1687–1702.

Wang, J., Liu, S., Haditsch, U., Tu, W., Cochrane, K., Ahmadian, G., Tran, L., Paw, J., Wang, Y., Mansuy, I., et al. (2003). Interaction of calcineurin and type-A GABA receptor gamma 2 subunits produces long-term depression at CA1 inhibitory synapses. J. Neurosci. *23*, 826–836.

Wills, Z.P., Mandel-Brehm, C., Mardinly, A.R., McCord, A.E., Giger, R.J., and Greenberg, M.E. (2012). The nogo receptor family restricts synapse number in the developing hippocampus. Neuron *73*, 466–481.

Zagrebelsky, M., Schweigreiter, R., Bandtlow, C.E., Schwab, M.E., and Korte, M. (2010). Nogo-A stabilizes the architecture of hippocampal neurons. J. Neurosci. *30*, 13220–13234.

Zagrebelsky, M., Godecke, N., Remus, A., and Korte, M. (2018). Cell type-specific effects of BDNF in modulating dendritic architecture of hippocampal neurons. Brain Struct Funct. *223*, 3689–3709.

Zemmar, A., Weinmann, O., Kellner, Y., Yu, X., Vicente, R., Gullo, M., Kasper, H., Lussi, K., Ristic, Z., Luft, A.R., et al. (2014). Neutralization of Nogo-A enhances synaptic plasticity in the rodent motor cortex and improves motor learning in vivo. J. Neurosci. *34*, 8685–8698.

Zemmar, A., Chen, C.C., Weinmann, O., Kast, B., Vajda, F., Bozeman, J., Isaad, N., Zuo, Y., and Schwab, M.E. (2018). Oligodendrocyte- and Neuron-Specific Nogo-A Restrict Dendritic Branching and Spine Density in the Adult Mouse Motor Cortex. Cereb. Cortex *28*, 2109–2117.

STAR★METHODS

KEY RESOURCES TABLE

REAGENT or RESOURCE	SOURCE	IDENTIFIER
Antibodies		
Mouse IgG1 anti-BrdU (Control)	Gift from M.E. Schwab (ETH and University of Zurich)	Kempf et al., 2014
Mouse IgG1 anti-Nogo-A	Gift from M.E. Schwab (ETH and University of Zurich)	Oertle et al., 2003
Goat anti-NgR1	R&D Systems	Cat# AF1440; AB_2183731
Rabbit anti-$GABA_AR$ γ2	Synaptic Systems	Cat# 224003; AB_2263066
Rabbit anti-$GABA_AR$ γ2	Alomone Labs	Cat# AGA-005; AB_2039870
Guinea pig anti-$GABA_AR$ γ2	Synaptic Systems	Cat# 224004; AB_10594245
Rabbit anti-$GABA_AR$ γ2 pSer327	Abcam	Cat# ab73183; AB_1268933
Guinea pig anti-$GABA_AR$ α2	Synaptic Systems	Cat# 224104; AB_10639393
Chicken anti-Synapsin1/2	Synaptic Systems	Cat# 106006; AB_2622240
Guinea pig anti-Gephyrin	Synaptic Systems	Cat# 147318
Rabbit anti-myc Tag	Thermofisher scientific	Cat# PA1-981; AB_325961
Rabbit anti-GluR1	Merck Millipore	Cat# AB1504; AB_2113602
Goat anti-Calnexin	SicGen antibodies	Cat# AB0037-200; 2333117
Rabbit anti-GAPDH	Sigma-Aldrich	Cat# G9545; AB_796208
Rabbit anti-VGAT (lumenal domain)	Synaptic Systems	Cat# 131103C3; AB_887867
anti-rabbit Cy2	Jackson Laboratories	Cat# 111-225-144; AB_2338021
anti-rabbit Cy3	Jackson Laboratories	Cat# 111-165-144; AB_2338006
anti-rabbit Cy5	Jackson Laboratories	Cat# 711-175-152; AB_2340607
anti-chicken Alexa Fluor® 488	Jackson Laboratories	Cat# 703-545-155; AB_2340375
Anti-chicken Cy5	Jackson Laboratories	Cat# 703-175-155; AB_2340365
anti-guinea pig Cy3	Jackson Laboratories	Cat# 706-166-148; AB_2340461
anti-rabbit HRP	Sigma-Aldrich	Cat# A0545; AB_257896
anti-mouse HRP	Sigma-Aldrich	Cat# A9044; AB_258431
anti-goat HRP	Jackson Laboratories	Cat# 305-035-003; 2339400
Chemicals, Peptides, and Recombinant Proteins		
JTE-013	Tocris	Cat# 2392
Nogo-A-Δ20	Gift from M.E. Schwab (ETH and University of Zurich)	Oertle et al., 2003
Tetrodotoxin citrate	Tocris	Cat# 1069
CNQX disodium salt	Tocris	Cat# 1045
Bicuculline methiodide	Tocris	Cat# 2503
Cyclosporine A	Tocris	Cat# 1101
EGTA	Sigma-Aldrich	Cat# E3889
Experimental Models: Organisms/Strains		
Wistar rats	Colony maintained at the animal facility of the University of Magdeburg	Charles River
C57BL/6J OlaHsd mice	Colony maintained at the animal facility of the TU Braunschweig	Harlan

(*Continued on next page*)

Continued

REAGENT or RESOURCE	SOURCE	IDENTIFIER
Recombinant DNA		
pK5_GABAR_6xmyc_γ2	Gift from J. Kittler (University College London)	Muir et al., 2010
pK5_GABAR_6xmyc_$\gamma2^{S327A}$	Gift from J. Kittler (University College London)	Muir et al., 2010
pCMV-GCaMP5G	Akerboom et al., 2012	Addgene Cat# 31788
Software and Algorithms		
Mini-Analysis	Synaptosoft Inc.	http://www.synaptosoft.com/MiniAnalysis/index.html
ImageJ	National Institutes of Health	https://imagej.nih.gov/ij/
MetaMorph	Molecular Devices	https://www.moleculardevices.com/products/cellular-imaging-systems/acquisition-and-analysis-software/metamorph-microscopy
XCellence Pro	Olympus	https://www.olympus-europa.com
Prism 5	GraphPad	https://www.graphpad.com/scientific-software/prism/
Axon pClamp 9	Molecular Devices	https://www.moleculardevices.com/products/axon-patch-clamp-system/acquisition-and-analysis-software/pclamp-software-suite#gref
EasyWin32	Herolab	https://www.herolab.de/index.php/de/gel-dokumentation/analyse-software.html
Andor iQ2	Oxford Instruments	https://andor.oxinst.com/products/iq-live-cell-imaging-software/andor-iq3
SynPAnal	Danielson and Lee, 2014	https://journals.plos.org/plosone/article?id=10.1371/journal.pone.0115298

LEAD CONTACT AND MATERIALS AVAILABILITY

Further information and requests for resources and reagents should be directed to and will be fulfilled by the Lead Contact, Marta Zagrebelsky (m.zagrebelsky@tu-bs.de).

This study did not generate new unique reagents.

EXPERIMENTAL MODEL AND SUBJECT DETAILS

Mice

In this study male and female C57BL/6J OlaHsd mice and Wistar rats were used. All procedures concerning animals were approved by the animal welfare representative of the TU Braunschweig and the LAVES (Oldenburg, Germany, Az. §4 (02.05) TSchB TU BS).

Primary mouse hippocampal culture

Primary hippocampal cultures were prepared from C57BL/6 mice at embryonic day 18 as previously described (Kellner et al., 2014; Zagrebelsky et al., 2018). The mouse embryos were removed from the uterus and decapitated. Under sterile conditions the upper half of the brain was dissected and kept in ice cold Gey's balanced salt solution (GBSS) supplemented with glucose and adjusted to pH 7.2. The dissociation of the hippocampus was achieved by incubation with Trypsin / EDTA at 37°C for 30 min and by subsequent mechanical dissociation. The cells were plated at a density of $3.5x10^4$ (live-cell labeling and immunofluorescence) or $7x10^4$ (Ca^{2+} imaging with GCaMP5) cells per well on poly-L-lysine coated coverslips. The cells were kept in Neurobasal medium (NB^-, #21103049, Thermo Fisher) supplemented with 2% B27, 11% N_2 and 0.5 mM Glutamax (NB^+) at 37°C, 5% CO_2 and 99% humidity.

Primary rat hippocampal culture

Primary rat hippocampal cultures were prepared from embryonic Wistar rats at embryonic day 18 as described previously (Banker, 1980; Frischknecht et al., 2008). In brief, after dissociation with trypsin the cell suspension was plated onto poly-L-lysine- (Sigma) coated 18 mm glass coverslips (Menzel-Glaeser, Braunschweig, Germany) at a density of 30,000 cells per coverslip. After incubation in Dulbecco's Modified Eagle Medium (DMEM) plus fetal bovine serum at 37°C for 1-2 h, five coverslips were placed into a 35 mm

Petri dish containing a 70%–80% confluent monolayer of astrocytes in neurobasal medium supplemented with B27 and 5 mM glutamine. The cultures were maintained in a humidified incubator at 37°C with an atmosphere of 95% air and 5% CO_2. At 3 DIV AraC was added to the cells to a final concentration of 1.4 μM.

Mouse organotypic hippocampal slice culture

Organotypic hippocampal cultures were prepared from postnatal day 5 (P5) C57BL/6 mice of either sex as described previously (Michaelsen-Preusse et al., 2014; Stoppini et al., 1991). The mice were decapitated and the hippocampi were dissected in ice-cold sterile Gey's balanced salt solution (GBSS). Transversal slices were cut using a tissue chopper (McIlwain) at a thickness of 400 mm. The slices were placed on Millicells CM membrane inserts (Millipore) and cultivated at 37°C, 5% CO2 and 99% humidity in a medium containing 50% BME (Eagle, with Hanks salts without glutamine), 25% Hank's Buffered Salt Solution (HBSS), 1% glucose, 25% donor equine serum (HyClone), and 0.5% L-glutamine. A mixture of antimitotic drugs (cytosine arabinoside, uridine, and fluorodeoxyuridine; 10^{-6} to 10^{-7} M each) was applied for 24 h 3 days after preparation.

Acute mouse hippocampal slices

Acute hippocampal slices were prepared from 6-8 weeks old C57BL/6 mice. The mice were euthanized with CO_2, decapitated and the brain was dissected and incubated for 3 min in 4°C carbogenated (95% O_2, 5% CO_2) artificial cerebrospinal fluid (ACSF) containing 125 mM NaCl, 2.5 mM KCl, 1.25 mM NaH_2PO_4, 2 mM $MgCl_2$, 26 mM $NaHCO_3$, 2 mM $CaCl_2$, and 25 mM glucose. The hippocampi were dissected and 400 mm thick transversal slices were cut with a Tissue Slicer (Stoelting). The slices were maintained at room temperature for at least 90 min in a submerged storage chamber with carbogenated ACSF before treatment.

METHOD DETAILS

Antibody and peptide treatment

The loss-of-function for the Nogo-A signaling was achieved by application of: a monoclonal Nogo-A specific, function-blocking antibody against an 18-aa peptide within the NiG-Δ20 domain, the most inhibitory region of Nogo-A (mouse IgG1 11C7; 5μg / mL gift from Martin Schwab, ETH and University of Zurich; Liebscher et al., 2005; Oertle et al., 2003); an antagonist of the sphingosine-1-phosphate receptor 2 (S1PR2; 5 μM JTE-013; Tocris) or a function-blocking antibody against the Nogo receptor NgR1 (5 μg/ml affinity-purified goat IgG anti-Nogo receptor; R&D Systems). A control mouse IgG1 (mouse IgG1 anti-BrdU, FG12, 5μg / mL, gift from Martin Schwab, ETH and University of Zurich) antibody was used as control for Nogo-A and NgR1 loss-of-function experiments. The gain-of-function for the Nogo-A NiG-Δ20 and Nogo-66 domains were obtained by application of the Δ20 (300 nM; Oertle et al., 2003, gift from Martin Schwab, ETH and University of Zurich) and P4 soluble peptides (4 μM; Alpha Diagnostic International). The boiled Δ20 and P4 peptides were used as controls in all experiments except for patch clamp recording, where PBS was used. For antibodies and peptides solved in DMSO, PBS or H_20 an equal amount of solvent was used as control. The treatments were applied as follows: 1) for patch clamp recording, single particle tracking and calcium imaging experiments: the application started right after the first time point acquisition and lasted until the end of the experiment. The different agents were diluted in ACSF (containing in mM 125 NaCl, 2.5 KCl, 26 $NaHCO_3$, 1.25 NaH_2PO_4, 2 $MgCl_2$*$6H_2O$, 2 $CaCl_2$*$2H_2O$, 25 D-glucose*H_2O; pH 7.4) saturated with carbogen and supplemented with 1 μM tetrodotoxin, 10 μM bicuculline (mEPSCs), 20 mM CNQX (mIPSCs) for patch clamp, in extracellular solution (145 mM NaCl, 10 mM Glucose, 10 mM HEPES, 5 mM KCl, 2 mM $CaCl_2$, 2 mM $MgCl_2$) for single particle tracking and in Hank's buffered salt solution (HBSS) for calcium imaging; 2) for live cell labeling the treatments were performed for 10 min right before fixation in a humidified incubator at 37°C with an atmosphere of 95% air and 5% CO_2. The agents were diluted in NB^- medium; 3) for the synapstosomes preparation for 10 min in ACSF (containing in mM 125 NaCl, 2.5 KCl, 26 $NaHCO_3$, 1.25 NaH_2PO_4, 2 $MgCl_2$*$6H_2O$, 2 $CaCl_2$*$2H_2O$, 25 D-glucose*H_2O; pH 7.4) saturated with carbogen.

Patch clamp electrophysiology

Somatic whole-cell recording was performed on visually identified pyramidal neurons in the CA3b area in 21 to 25 DIV organotypic mouse hippocampal slice cultures. The slices were transferred to an open imaging chamber at 32°C, continuously perfused (1 mL/min) with ACSF (containing in mM 125 NaCl, 2.5 KCl, 26 $NaHCO_3$, 1.25 NaH_2PO_4, 2 $MgCl_2$*$6H_2O$, 2 $CaCl_2$*$2H_2O$, 25 D-glucose*H_2O; pH 7.4) saturated with carbogen and supplemented with 1 μM tetrodotoxin, 10 μM bicuculline (mEPSCs), 20 mM CNQX (mIPSCs). The antibodies and peptides were diluted in ACSF at the stated concentrations (see antibody and peptide treatment section). The slices were let to adapt for 20 min before starting the recording. Glass pipette electrodes (resistance: 4.0-6.5 MΩ) were pulled with a PC-10 vertical micropipette puller (Narishige) from borosilicate capillaries (1.5 mm). The pipette internal solution contained (in mM) 70 K-gluconate, 70 KCl, 10 HEPES, 0.5 EGTA, 4 MgATP, 0.4 NaGTP and 4 Na_2phosphocreatine (pH 7.3). Patching was performed under a Zeiss (Axioskop 2 FS Plus) microscope using a 40X water-immersion objective (0.8 NA). Cells were voltage-clamped at −70 mV and mIPSCs and mEPSCs were recorded every 5 min for 120 s up to 30 min after starting antibody application. Input resistance (R_{in}) and series resistance (R_s) were monitored throughout the recordings and only stable cells (< 20% change in R_{in} and R_s) with R_{in} > 100 MΩ and R_s < 25 MΩ were included in the analysis. Signals were amplified using a Multiclamp 700B amplifier (Molecular Devices) and digitized with a Digidata 1322A digitizer (Molecular Devices). Data analysis was performed with Mini Analysis

software (Justin Lee). The data are presented as mean ± standard error of the mean (SEM). Statistical analysis was performed in Prism (GraphPad) using a Two-Way ANOVA with Sidak's multiple comparison post hoc test.

Transfection of primary hippocampal neurons

At 21 DIV, cultured mouse hippocampal neurons were transfected with 0.8 μg of the DNA expression plasmid for $GABA_AR$ γ2-myc or $GABA_AR$ $\gamma2^{S327A}$-myc under a CMV promoter (Muir et al., 2010) using Lipofectamine® 2000 transfection reagent (ThermoFisher Scientific). The transfection mix was prepared in NB- and given to the cells for 40 min in a humidified incubator at 37°C with an atmosphere of 95% air and 5% CO_2.

Live-cell labeling and immunofluorescence

Live-cell labeling of surface $GABA_A$ receptors was performed in 21-25 DIV primary mouse hippocampal cultures. The neurons were incubated with the primary antibodies against $GABA_AR$ γ2 (1:500, #22403, Synaptic Systems) or anti-$GABA_AR$ α2 (1:500, #224104, Synaptic Systems) diluted in NB^- medium containing 1% BSA for 10 min at 37°C, 5% CO_2 and 99% humidity. In experiments where cyclosporine A was used to inhibit calcineurin activity, or EGTA for Ca^{2+} chelation the cells were incubated with anti-$GABA_AR$ γ2 antibody in NB^- medium containing 1% BSA, 1 μM cyclosporine A or 2mM EGTA for 20 min at 37°C. Subsequently the cells were treated with either the specific inhibitors or the respective controls (see Antibody and Peptide Treatment section) diluted in NB^- medium for 10 min at 37°C (in CaN activity experiments 1 μM cyclosporine A and for EGTA experiments 2mM were additionally added). At the end of the treatment the cells were fixed with 4% paraformaldehyde (PFA) in PB for 10-15 min at RT. Cells were then permeabilized with 0.3% Triton X-100 in PBS for 5 min and unspecific binding was blocked with 2% BSA in PBS for 30 min. For post hoc immunofluorescence, the fixed neurons were incubated with anti-synapsin (1:1,000, #106006, Synaptic Systems), anti-gephyrin (1:500, #147318, Synaptic Systems), anti-$GABA_AR$ γ2 pSer327 (1:500, #ab73183, Abcam) or Myc-Tag (1:100, #PA1-981, ThermoFisher) diluted in PBS containing 2% BSA for 1 h followed by an incubation with the following secondary antibodies (1:500, Jackson Laboratories): anti-rabbit Cy2 (#111-225-144), anti-rabbit Cy3 (#111-165-144), anti-rabbit Cy5 (#711-175-152), anti-chicken Alexa Fluor® 488 (#703-545-155), anti-chicken Cy5 (#703-175-155), anti-guinea pig Cy3 (#706-166-148) diluted in PBS for 40 min. Finally, the cells were incubated in a quenching solution containing 50 mM NH_4Cl_2 in PBS for 10 min and mounted with Fluoro-Gel (Electron Miscroscopy Sciences) onto glass slides for imaging.

Widefield fluorescence imaging and analysis

2D images were acquired using an upright Axio Imager M2 microscope (Zeiss) equipped with an oil-immersion objective (63x NA 1.4) and a CCD camera. Primary dendrites of fluorescently labeled and isolated neurons were randomly chosen. Cells from a single culture preparation were imaged with the same sub-saturation exposure time. Background fluorescence of 2D images was determined in ImageJ (National Institutes of Health) by placing ROIs on the dendrite of interest where no synaptic protein fluorescence was visible. The mean gray value of all ROIs per dendrite was averaged and used as background in further analysis of this cell. Puncta density and fluorescence intensity of synaptic proteins was detected in SynPAnal (Danielson and Lee, 2014) after subtraction of 2x background. In all cases the colocalization with synapsin-positive puncta was defined by overlap of at least 1 pixel after 2x background subtraction and was quantified in ImageJ. All analyses were performed by an experimenter blind to the treatment.

Single particle tracking and Fluo-4 imaging

$GABA_AR$ primary antibodies were tagged with quantum dots by mixing anti-$GABA_AR$ antibodies (1:10, #22403, Synaptic Systems), F(ab')2-goat anti-rabbit IgG Qdot655 (1:10, #Q11422MP, Thermo Fisher) and 10x casein solution (1:10, #SP-5020, Vector Laboratories) in PBS and vortexing for 10 min at RT. 10-14 DIV primary rat hippocampal neurons were incubated with a fluorescent (Oyster-550) labeled anti-VGAT antibody (lumenal domain, 1:200, #131103C3, Synaptic Systems) in extracellular solution (145 mM NaCl, 10 mM Glucose, 10 mM HEPES, 5 mM KCl, 2 mM $CaCl_2$, 2 mM $MgCl_2$) containing 0.5% BSA for 30 min at 37°C followed by incubation with the QD-$GABA_AR$ antibody mix (1:200) diluted in extracellular solution containing 0.5% BSA for 5 min at 37°C. Labeled cells were washed in extracellular solution containing 0.5% BSA before imaging. Coverslips were moved to a closed imaging chamber filled with extracellular solution at 37°C. Recording was performed under an upright Olympus BX61 microscope equipped with a spinning disk (Yokogava) and a 100x oil-immersion objective (NA 1.4), using the 561 nm laser line and appropriate emission filters to record consecutive images of synapse labeling and QD tagged $GABA_A$-receptors. Images were captured by an EMCCD camera (iXon+ 897, Andor Technology). The imaging system was controlled by the Andor iQ2 software. Image sequences of 1000 frames and acquisition rate of 33 Hz were recorded for QD labeled $GABA_A$Rs and 100 frames (33 Hz) were acquired for VGAT labeled synapses. The QD-$GABA_AR$ tracking was repeated every 5 min for up to 20 min.

The mean explored surface of QD-$GABA_A$Rs was examined in ImageJ. Briefly, maximum projections of 1000 frames recordings before and 10 min after control or Nogo-A neutralizing antibody application were generated. After background subtraction, the projections were binarized and the explored surface was quantified by the "Analyze Particles" function (0.1-Inf μm^2, no circularity). The data are then presented as explored average surface of QD-labeled $GABA_AR$.

QD-GABA$_A$R diffusion dynamics were analyzed using the PalmTracer plugin for MetaMorph software (Universal Imaging). In detail, VGAT fluorescence was averaged over 100 frames, background fluorescence was subtracted and VGAT positive areas were marked as synaptic compartments. Throughout the text and figures, all data marked with "synaptic" correspond to QD-labeled GABA$_A$R found in VGAT labeled spots. Localization of QDs was carried out using a wavelet-based algorithm. Trajectories of QD-tagged GABA$_A$Rs were reconstructed by a simulated annealing algorithm (Izeddin et al., 2012). The diffusion coefficient (D), defined as a measure for the random motion of GABA$_A$R within the cellular membrane based on the surface they explored over time was generated by a linear fit of the first 4 points of the mean square displacement (MSD) over time using $MSD(t) = < r^2 > (t) = 4Dt$. Trajectories shorter than 8 points were not include into the analysis. The blinking of QDs was not taken into account for the reconstruction of trajectories, all shorter trajectories were rejected and not further analyzed. For MSD plots we averaged the MSDs generated from trajectories with $\geq$ 34 points (1 s, Figure S2). The confinement area of GABA$_A$Rs in the membrane was calculated by fitting the MSD according to the procedure described by Kusumi et al. (1993).

In experiments where QD-SPT was paired with Ca^{2+} imaging, neurons were incubated with Fluo-4 AM (0.5 μM, #F14201, Fisher Scientific) together with the antibody coated QD-anti-GABA$_A$R γ2 in extracellular solution containing 0.5% BSA for 5 min at 37°C. Fluo-4 fluorescence was imaged within the dendrites of the labeled cells in sequences of 1000 frames at 33 Hz every 5 min for up to 20 min. Fluo-4 fluorescence analysis was performed in ImageJ (National Institutes of Health) by averaging fluorescence intensity over 1000 frames after background subtraction. The ratio of fluorescence intensities (F/F_0), where F is a fluorescence intensity and F_0 is the intensity at the first time point, was assessed by normalization to the first time point of each experiment. Statistical analysis was performed in Prism (GraphPad7) using a Two-Way repeated-measures ANOVA followed by a Bonferroni post-test. Correlation between diffusion dynamics and Fluo-4 intensity of single cells was tested using a Spearman test. All analyses were performed by an experimenter blind to the treatment.

Ca^{2+}-imaging

Primary mouse hippocampal neurons were transfected with GCaMP5g expression plasmid using Lipofectamine 2000 (Invitrogen) at DIV20-25. One day after lipofection coverslips were moved to a recording chamber filled with Hank's buffered salt solution (HBSS) and let rest for 30 min at RT. Imaging of randomly chosen GCaMP5g expressing neurons was performed using a 40x objective (LUMPLFLN W, NA 0.7) with an Olympus fluorescence Microscope BX61WI, equipped with a CCD camera. Time lapse recordings of 500 frames at 5 Hz were acquired using XCellence pro imaging software. The coverslips with the transfected cells were incubated in a recording chamber filled with HBSS for 30 min to adjust. A continuous flow of the HBSS solution was achieved using a peristaltic pump and kept at a constant speed of 1 mL/min. The neurons were treated with the antibodies and peptides (Figures 5A–5C, see Antibody and Peptide Treatment section) diluted in HBSS at RT. For treating the cells with the different antibodies another HBSS solution was prepared separately with a final concentration of 5 μg/ml. The cells were imaged twice before and four times after starting the treatment at an interval of ten minutes.

Analysis of the data was performed using ImageJ software. The region of interest (ROI) used in the image analysis was chosen to correspond to dendritic spines or the cell body. For the whole duration of the treatment always the same spines were observed. An additional ROI was drawn for background correction. To calculate the change in fluorescence intensity the following equation was used: $\Delta F/F_0 = [(F-B)-(F_0-B_0)] / (F_0-B_0)$, where F_0 and B_0 represent the mean gray value of the selected ROIs at resting conditions. The amplitude and frequency of the transients were averaged for each spine of one cell. Data were normalized to the first recording before wash-in of the antibodies and peptides. For statistical analysis a repeated-measures ANOVA was performed. To test whether the assumption of sphericity is violated within the treatments, the Mauchly's test was done, followed by a Greenhouse-Geisser correction if sphericity has been violated. Further a paired Student's t test was used to test for significances between the different treatments. All analyses were performed by an experimenter blind to the treatment.

Synaptosome isolation

The synaptosome isolation procedure was adapted from Suresh and Dunaevsky, (2015). Briefly, acute hippocampal slices were treated with control antibody, Nogo-A neutralizing antibody (5 μg/ml) or KCl (55 mM) in carbogenated ACSF at RT for 10 min and subsequently transferred to a medium containing 0.32 M sucrose, 5 mM HEPES (pH 7.5), 0.1 mM EDTA (pH 8.0) and Complete protease inhibitor cocktail pellet (Roche, 1 tablet per 50 mL). The slices were homogenized with a hand held homogenizer (DWK Life Sciences) on ice for 1 min. After centrifugation at 1,500 rpm at 4°C for 10 min the supernatant containing suspended synaptosomes was spun down at 13,500 rpm at 4°C for 20 min. The synaptosomes were lysed in RIPA buffer containing (50 mM TRIS, 150 mM NaCl, 2 mM EGTA, 1% Triton X-100, 0.25% DOC, pH7.5) on a rotor at 4°C for 30 min. Protein concentration was assessed by Bradford assay.

Western blot analysis

Protein samples were prepared for western blot analysis by adding SDS and β-mercaptoethanol. 20 μg of proteins were loaded and separated on 4%–12% polyacrylamide gradient gels followed by blotting onto nitrocellulose membranes using a semidry or tank blot. The membranes were blocked with 5% milk in TBS-Tween for 1 h at room temperature and incubated at 4°C overnight with the

following primary antibodies diluted in TBS-Tween: anti-GluR1 (1:1,000, #AB1504, Merck Millipore), anti-Nogo-A (5 μg/ml, 11C7, gift from Martin Schwab, ETH Zurich), anti-GAPDH (1:15,000, #G9545, Sigma-Aldrich). The membrane was washed in TBS-Tween and incubated for 1 h at room temperature with the anti-mouse (1:20,000, #A9044, Sigma-Aldrich), anti-rabbit (1:20,000, #A0545, Sigma-Aldrich) or anti-goat (1:20,000, #305-035-003, Jackson Laboratories) secondary antibodies conjugated with HRP. Immunoreactivity was detected on an X-ray film by chemoluminescence (Luminata Crescendo Western HRP substrate, Millipore) and densitometry of bands was conducted in EasyWin32. A Student's t test was used to assess differences between treatments.

DATA AND CODE AVAILABILITY

This study did not generate/analyze any datasets/code.